Temple University

Annual Progress Report: 2009 Formula Grant

Reporting Period

July 1, 2010 – June 30, 2011

Formula Grant Overview

Temple University received $2,375,033 in formula funds for the grant award period January 1, 2010 through December 31, 2013. Accomplishments for the reporting period are described below.

Research Project 1: Project Title and Purpose

The Anabolic Role of Cannabinoid Receptors in Bone - The goal of the planned project is to define the anabolic role of cannabinoid receptors in bone. Recent studies have demonstrated the presence of endocannabinoids and their G protein-coupled cannabinoid receptors, CB1 and CB2, in the skeleton. Although it has become clear that this system is functional in bone, the precise mechanisms of action are only beginning to emerge. The planned studies will generate new information regarding the anabolic effects of cannabinoid receptors and mechanisms of action on osteoblast differentiation and function. Once we understand how cannabinoid receptors function to promote bone formation, this information will be helpful in developing new therapeutic strategies to selectively enhance bone formation in patients with clinically significant bone loss.

Duration of Project

7/1/2010 – 6/30/2011

Project Overview

The goal of the project is to define the anabolic role of cannabinoid receptors in bone. Recent studies have demonstrated the presence of endocannabinoids and their G protein-coupled cannabinoid receptors CB1 and CB2 in the skeleton. Although it has become clear that this system is functional in bone, the precise mechanisms of action are only beginning to emerge. We have found that bone mass is significantly reduced in CB1/CB2 double receptor knockout (CB1/2 dKO) mice. To examine the functional significance of CB1 and CB2 receptors on osteoblast differentiation, we established primary osteoblast cultures utilizing newborn wild-type calvaria. Measurement of alkaline phosphatase (ALP) activity was assessed to evaluate the effects of specific CB receptor antagonists on osteoblast differentiation. Treatment with a CB1 antagonist or a CB2 antagonist caused a significant, dose-dependent inhibition of ALP activity. When cultures were treated with both CB receptor antagonists simultaneously, the inhibition of ALP activity was more pronounced compared to either antagonist alone. *Our results suggest that both CB1 and CB2 are functional receptors during osteoblast differentiation in vitro and in*

the regulation of bone mass in vivo. The observation that combined CB1 and CB2 receptor antagonism/deletion has a more dramatic effect compared to single receptor deletion warrants additional studies to evaluate intracellular signaling subsequent to ligand activation of CB1 and CB2 in osteoblasts.

In this project, we will characterize the mechanisms underlying this response by using a combination of pharmacological and genetic tools to identify the receptors involved. The effects of cannabinoid agonists, antagonists/inverse agonists and related compounds on osteoblast proliferation, apoptosis and differentiation will be compared in cultures prepared from WT, CB1 KO, CB2 KO and CB1/2 dKO mice. We will also identify the response of two key intracellular signaling pathways (ERK and Akt) to the most efficacious agents (using Western blot analysis and immunocytochemistry). Transcriptional activation of Osterix will be assessed by Runx2 activation of the Osterix gene promoter using CHIP assays. These experiments will provide insights into the role that the CB receptors play in regulating bone mass and into potential signaling mechanisms whereby CB receptors regulate osteoblast differentiation and function. Results from these studies could potentially be used to develop anabolic therapeutic agents for bone disease.

Principal Investigator

Mary E. Abood, PhD
Associate Professor
Temple University School of Medicine
Department of Anatomy and Cell Biology
3500 North Broad Street
Philadelphia, PA 19140

Other Participating Researchers

Jahan P. Marcu, BS - employed by Temple University

Expected Research Outcomes and Benefits

It has recently been discovered that endocannabinoids and their G protein-coupled cannabinoid receptors type 1 (CB1) and type 2 (CB2) are present in the skeleton. In addition, polymorphisms in the CB2 gene are associated with osteoporosis. Although it has become clear that this system is functional in bone, the precise mechanisms of action are only beginning to emerge. We have found that both receptors are important for bone development in vivo and osteoblast differentiation in vitro; and furthermore, that there is a synergistic interaction between these two receptors. In this project, we expect to identify CB1- and CB2-mediated responses involved in osteoblast differentiation. Data from the studies will help explain the importance of signaling cascades from cannabinoid receptors (CB1 and CB2) during normal bone development and maintenance, as well as contribute to providing a mechanism for the CB1/2 double KO bone phenotype. The identification of cannabinoid compounds with an anabolic effect on bone could potentially be used to develop therapeutic strategies for treating various forms of osteopenia and

to accelerate bone formation in situations (e.g., fracture healing, distraction osteogenesis) where such intervention would have a favorable clinical outcome.

Summary of Research Completed

The Anabolic Role of Cannabinoid Receptors in Bone - The goal of the planned project is to define the anabolic role of cannabinoid receptors in bone. Recent studies have demonstrated the presence of endocannabinoids and their G protein-coupled cannabinoid receptors, CB1 and CB2, in the skeleton. Although it has become clear that this system is functional in bone, the precise mechanisms of action are only beginning to emerge. The planned studies will generate new information regarding the anabolic effects of cannabinoid receptors and mechanisms of action on osteoblast differentiation and function. Once we understand how cannabinoid receptors function to promote bone formation, this information will be helpful in developing new therapeutic strategies to selectively enhance bone formation in patients with clinically significant bone loss.

Specific Aims:
1) To determine intracellular signaling subsequent to ligand activation of CB1 and/or CB2 receptors in osteoblasts by using a combination of pharmacological and genetic tools to identify the receptors involved. The effects of cannabinoid agonists, antagonists/inverse agonists and related compounds on osteoblast proliferation, apoptosis and differentiation will be compared in cultures prepared from WT, CB1 KO, CB2 KO and CB1/2 dKO and GPR55 KO mice.

2) To identify the response of two key intracellular signaling pathways (ERK, and Akt) to the most efficacious agents (using Western blot analysis and immunocytochemistry).

Progress towards aims:
Specific Aim 1. To examine the functional significance of CB1 and CB2 receptors on osteoblast differentiation, we established primary osteoblast cultures utilizing newborn wild-type calvaria. Measurement of alkaline phosphatase (ALP) activity was assessed to evaluate the effects of CB1/CB2 receptor deletion (CB1/2 KO mice) on osteoblast differentiation. As shown in Figure 1, osteoblasts prepared from CB1/2 KO mice exhibited less differentiation than those prepared from WT mice, as documented by ALP staining (A,B) and activity (C,D). In Figures 1A and 1B, primary osteoblasts were isolated from the calvaria of 3-5 day old mice and stained for ALP activity. The images provide a qualitative assessment of matrix mineralization. The ALP staining was much more intense in wild type (WT) osteoblasts compared to the cells from CB1/2 KO animals. In Figure 1C, matrix levels of ALP were slightly lower in the CB1/2 KO primary osteoblasts than in WT, corroborating staining results. However, a defect in osteoblast differentiation could result in the ALP enzyme being released at high rates into media or serum, resulting in lower staining and matrix levels. Serum ALP activity was not significantly different between WT and CB1/2 KO cells. This suggests that there is less ALP production in CB1/2 KO mature osteoblasts.

Next, the ability of WT rat primary osteoblasts to proliferate in the presence of CB1 and CB2 receptor antagonists was assessed. As shown in Figure 2, treatment with a CB1 antagonist (SR141716) or a CB2 antagonist (SR144528) caused a significant, dose-dependent inhibition of cell proliferation.

Under low serum conditions the CB1 antagonist SR141716 was able to significantly reduce absorbance of proliferating osteoblasts (a measure of cell proliferation) within 48 hours (Fig 2A). The CB2 antagonist did not significantly alter cell proliferation in primary osteoblasts (Fig 2B). When applied in combination, the antagonists reduced cell proliferation similar to the application of the CB1 antagonist alone. Under normal conditions (no differentiation factors) CB1/2 KO osteoblasts isolated from 3-5 day old mice produced a significantly higher amount of proliferation compared to WT (Fig 2D). However, this effect was reversed when the cells were challenged with differentiation factors (Fig 2E). The results indicate that there may be a defect in cell proliferation during maturation of osteoblasts isolated from CB1/2 KO animals.

Specific Aim 2. To identify the response of two key intracellular signaling pathways (ERK, and Akt) to the most efficacious agents (using Western blot analysis and immunocytochemistry).

Cannabinoid receptors signal in bone: CB1, CB2, and GPR55. In Figure 3A, the effect of the CB1 antagonist SR141716 was examined in the MC3T3 osteoblastic cell line. In figure 3A, a representative western blot of a SR141716 timecourse for pERK is shown. Blockade of the CB1 receptor with SR141716 produced a rapid increase in the activity of pERK which returned to near basal levels after about 1 hour. Blockade of the CB2 receptor did not cause a noticeable difference in ERK activity (Figure 3B). The putative cannabinoid receptor GPR55 was targeted with the agonist lysophosphatidylinositol (LPI), which caused a small increase in pERK activity, which did not appear to return to baseline even after 3 hours (Figure 3C).

Nonpsychotropic Cannabinoids May Alter ERK and AKT. Activation of CB1 receptors is largely responsible for the psychotropic effects of marijuana and delta-9-tetrahydrocannabinol (THC). We wanted to investigate whether nonpsychotropic agonists may stimulate signaling pathways important for bone growth; these compounds would be more desirable for further therapeutic development in the treatment of bone diseases. Interestingly, we found the CB2-selective agonist, HU308, was able to stimulate pERK activity (Fig. 4A). This suggests that activation of the CB2 receptor may be beneficial for bone growth, in line with our observations that receptor antagonists did not affect cell proliferation. The nonpsychotropic plant cannabinoid agonist, cannabidiol, stimulated pAKT activity (Fig 4B).

THC May Alter ERK Activity. Shown in figure 5 is a representative western blot from a 2 hour timecourse of pERK activation following treatment of the MC3T3 osteoblast cell line. THC stimulated pERK activity until about 45 minutes, where activity began to noticeably drop off. THC and other synthetic cannabinoids remain the most highly abused illicit narcotics. Investigating the effect of compounds such as THC, may provide information for identification of bone disorders due to the abuse of cannabinoid drugs, potentially allowing effective interventions in drug abusing populations.

Recently, an interest in the role of endogenous cannabinoid signaling in bone has surfaced. Non-psychotropic cannabinoids, such as CBD and HU308 may have the potential to treat a wide variety of bone pathologies, without the negative effects of THC. However, THC and other synthetic cannabinoids remain the most highly abused illicit narcotics. We have begun investigating the effects of endogenous, non-psychotropic, and widely abused cannabinoids on

the signaling cascades in bone. We sought to elucidate molecular mechanisms of cannabinoid on bone. To study the role of endogenous cannabinoids, we used CB1 and CB1 antagonists.

Additionally, we isolated primary osteoblasts from WT and CB1/2 KO neonatal pups, and examined the cells for alterations in ALP staining and cell proliferation. Our data may lead to: a better understanding of bone biology, may aid with drug development for bone diseases, and may provide information for identification of bone disorders due to the abuse of cannabinoid drugs, potentially allowing effective interventions in drug abusing populations.

Materials and Methods:

Osteoblast Isolation and Culture

Primary immature osteoblasts were isolated from the calvaria bones of 3-5 day old animals by sequential collagenase digestions. Prior to experiments, the cells were cultured in a 75cm^2 flask in standard α-MEM media. The cells were left to adhere and proliferate until the flask was nearly confluent before using in experiments.

Proliferation Assays with Primary Osteoblasts

Primary cells from rats were plated at 2,000 cells/well in MEM with 10% FBS. After 24 hours the cells were washed with plain media, and the media was replaced with MEM with 1% FBS and cells were treated with 1,3,5,7 and 10 µM of SR141716A, SR144528, or a combination of the two compounds. Cells culture was stopped at 24 and 48 hours post treatment. Cell proliferation was measured using a WST-1 proliferation kit from Caymen (Cat# 10008883).
To measure the number of mature osteoblasts, primary cells from WT and CB1/CB2 KO mice were plated at 2,000 cells/well in 96 well plates. After 24 hours the media was replaced with MEM containing β-glycerol phosphate (10mM) and ascorbic acid (50ug/ml). The media with differentiation factors was changed every 2-3 days. After 14 days, the proliferation differentiated or mature osteoblasts were measured number using a WST-1 proliferation kit from Caymen (Cat# 10008883). To measure the proliferation in undifferentiated ostoeblasts, primary cells from WT and CB1/CB2 KO mice were plated at 4,000 cells/well in 96 well plates in 2.5% FBS. After 48 hours, the media was removed and cell proliferation was measured using a CyQuant kit from Invitrogen (Cat# C35006). A calibration curve was also generated to determine cells numbers (Data not shown).

ALP staining

Primary immature osteoblasts were seeded at 100,000 cells/well into 12 well plates. After 24 hours the media was replaced with MEM containing β-glycerol phosphate (10mM) and ascorbic acid (50 µg/ml). The media with differentiation factors was changed every 2-3 days. After 14 days, the cells were washed and stained for alkaline phosphatase using the ALP staining kit from Sigma-Aldrich (Cat# 86R-1KT).

ALP activity

Media and cell lysates from 96 well plates were analyzed for ALP activity after 14 days of differentiation with the LabAssay ALP kit from Wako (Cat# 291-58601).

Time course experiments

MC3T3 cells were seeded into 10mm dishes at 200,000 cells/dish in MEM with 10% FBS. The cells were transferred to 1% FBS at least 24 hours prior to experimentation. Cells were washed with HBSS before receiving 1 µM of a cannabinoid (dissolved in DMSO) in HBSS. Cells were harvested at various times using a protease (Thermo Sci Cat#78425) and phosphatase (Thermo Sci Cat#78420) inhibitor cocktail.

Westerns

Protein content of cellular extracts was determined using Bradford reagent and an identical amount of protein from each extract was analyzed on 10% polyacrylamide gels for SDS-page analysis. Levels of pERK and ERK were determined using a monoclonal antibody (1:5000 Sigma-Aldrich M8159) and a polyclonal antibody (1:1000; Cell Signaling 9102). AKT was determined using a polyclonal antibody (1:1000 dilution; Cell Signaling Cat#9275). The levels RUNX2 were determined with a polyclonal antibody (1:200; Santa Cruz BioTech Cat#10758). Membranes were incubated with the appropriated primary and secondary antibodies (Odyssey Cat# 926-32210, 926-32221, and 926-32211) and analyzed on a LICOR machine to generate integrated intensity values of activated proteins. Background levels of inactivated ERK or actin were used as a control for each individual value.

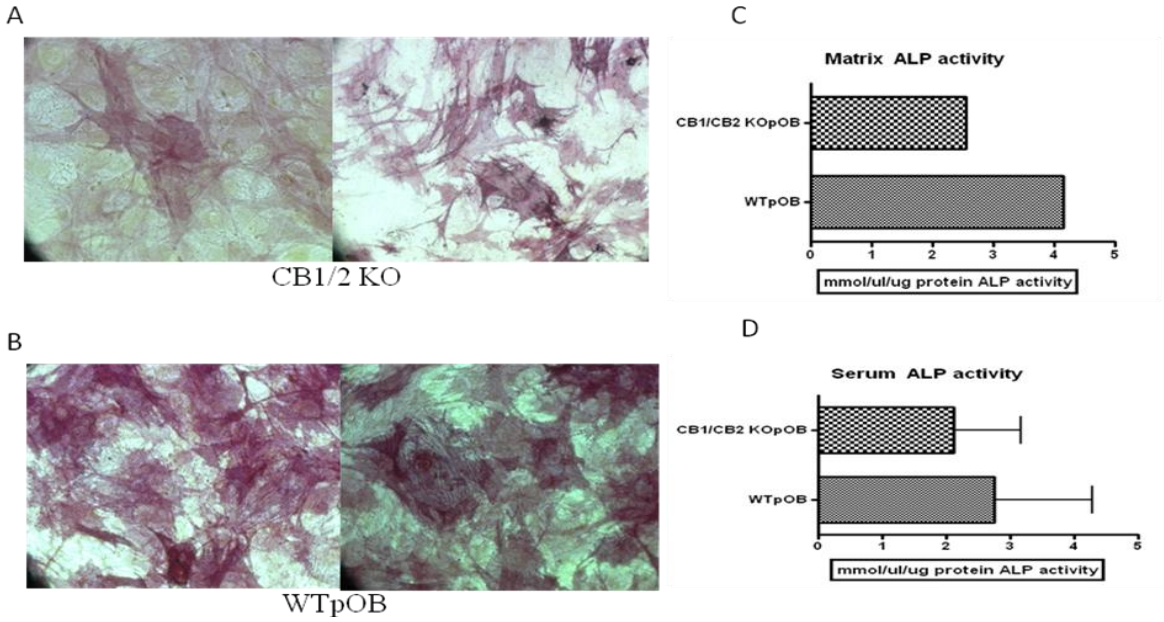

Figure 1. ALP Staining and ALP activity in Primary Osteoblasts prepared from KO or WT mice

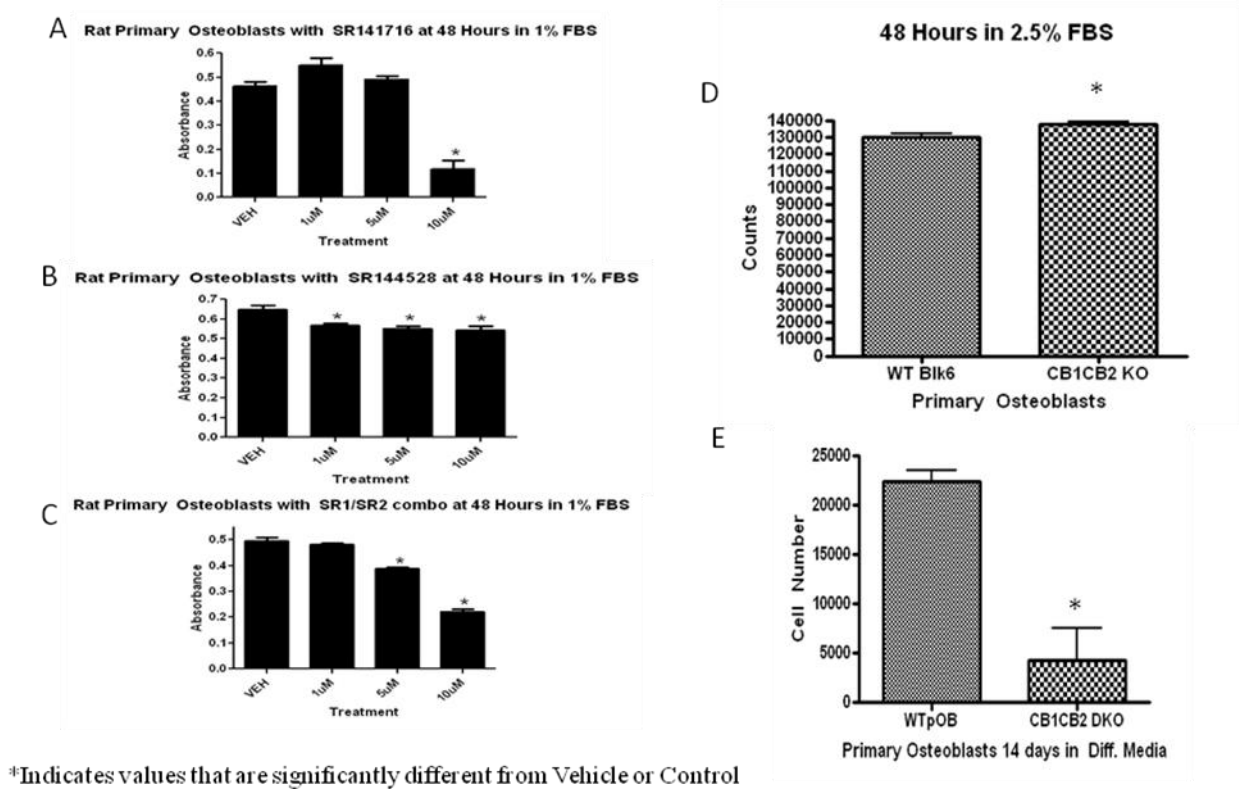

Fig 2. Cell Proliferation experiments in Primary Osteoblasts

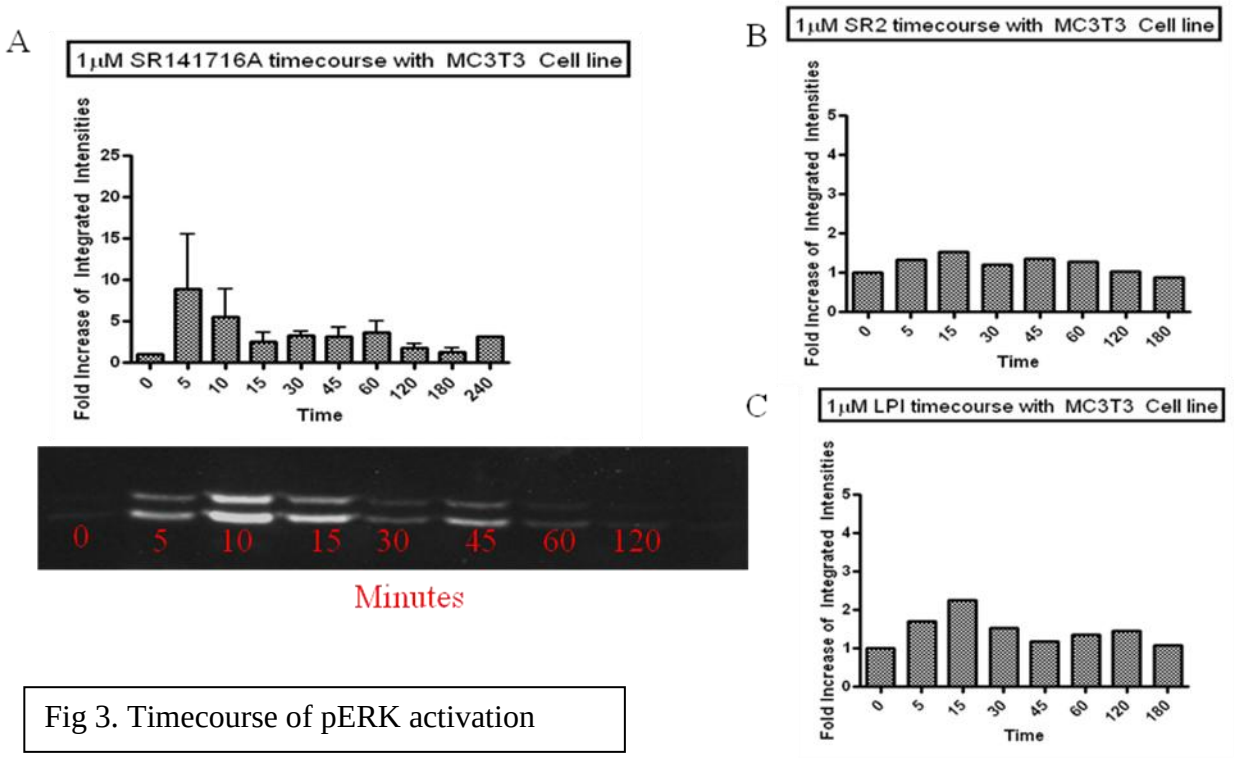

Fig 3. Timecourse of pERK activation

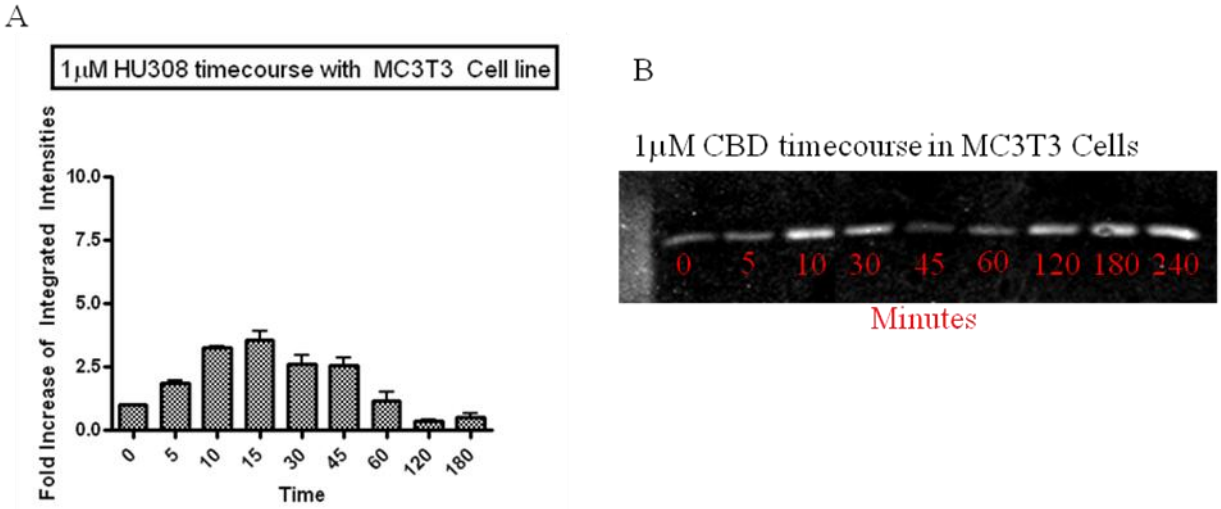

Figure 4. Non-psychotropic cannabinoids alter ERK and AKT activity

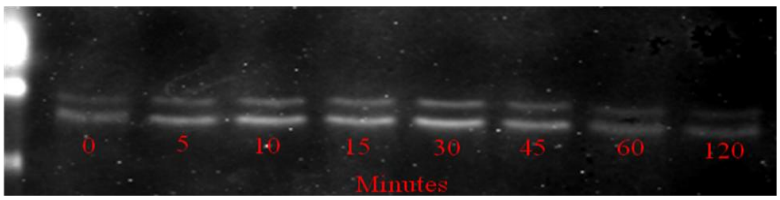

Figure 5. 1 µM THC activates pERK in MC3T3 osteoblasts cells

Research Project 2: Project Title and Purpose

Effects of IL-19 on Endothelial Cell Activation and Angiogenesis - Cardiovascular disease is the number one killer of Americans. Vascular diseases such as atherosclerosis, and hypertension are inflammatory in nature. Very little has been reported on the potential protective effects of anti-inflammatory cytokines on development of vascular disease. We have novel preliminary data which shows that the naturally occurring anti-inflammatory compound, Interleukin-19 (IL-19) can have stimulatory effects on endothelial cells grown in culture. The purpose of this project is to determine if IL-19 can have pro-angiogenic effect in vivo.

Anticipated Duration of Project

7/1/2010 – 12/31/2013

Project Overview

Endothelial cell paracrine and autocrine activation can result in migration and proliferation, and is an essential component of multiple normal and pathophysiological processes including atherosclerosis, permeability, wound healing, and angiogenesis. Angiogenesis is the growth of new blood vessels and normally occurs in the process of healing wounds and restoring blood flow after injury or insult, and many inflammatory cytokines play an important role in angiogenesis. Although both inflammatory and anti-inflammatory cytokine expression are an essential part of wound healing, the role of anti-inflammatory interleukins in initiation and progression of angiogenesis are less clear. Many vascular diseases, such as atherosclerosis and hypertension, are inflammatory in nature. Although a great deal of attention has been given to the role and effects of pro-inflammatory cytokines, very little has been reported on the potential protective effects of anti-inflammatory cytokines on the vascular response to injury, particularly with respect to direct effects on vascular smooth muscle cell (VSMC) pathophysiology. IL-19 is a newly described member of the IL-10 family of anti-inflammatory cytokines. We are the only laboratory to publish concerning the expression or presumed function of IL-19 in VSMC pathophysiology or a role in modulation of vascular diseases.

We have preliminary data which indicate that IL-19 is not present in normal endothelial cells (EC), but can be expressed in response to inflammation and injury. IL-19 expression is increased in neo vessels, and addition of IL-19 to cultured EC stimulates their growth and migration.

Despite this information NO studies on in vivo effects of IL-19 on development of angiogenesis have been reported. We have recently generated an IL-19 knock out mouse. We hypothesize that mice which lack IL-19 have reduced angiogenesis. In Aim 1 we will determine if there will be

decreased development of angiogenesis in IL-19 knock out mice subject to hind-limb ischemia. In Aim 2, we will determine if these mice have a reduced capacity to form microvessels toward matrigel plugs.

Principal Investigator

Michael Autieri, PhD
Associate Professor
Temple University School of Medicine
1050 MERB
3500 N. Broad Street
Philadelphia, PA 19140

Other Participating Researchers

Ross England, BS - employed by Temple University

Expected Research Outcomes and Benefits

Angiogenesis is the growth of new blood vessels and normally occurs in the process of healing wounds and restoring blood flow after injury. It is well known that many pro-inflammatory cytokines are pro-angiogenic. Very little is known about the effects of anti-inflammatory cytokines on the development of angiogenesis. IL-19 is a compound which occurs naturally in humans and functions to modify inflammatory cells and dampen the immune response. We have previously shown that IL-19 is induced in endothelial cells under inflammatory and pro-angiogenic conditions. Cultured EC in which IL-19 is added display pro-angiogenic effects, such as increased migration, proliferation, and tube formation. In this project, one outcome we expect is that mice, genetically deficient in IL-19, will have decreased angiogenesis. If these experiments are successful, then at least one major benefit of this research is that IL-19 could represent a new class of naturally occurring therapy to increase wound healing and improve outcome of ischemic vascular diseases.

Summary of Research Completed

<u>In Aim 1</u> we will determine if there will be decreased development of angiogenesis in IL-19 knockout mice compared with wild-type mice, subject to hind-limb ischemia.

Revascularization responses in the different strains of mice will be quantitatively assessed in the mouse hind limb ischemic assay. Our rationale for using the mouse hind limb ischemia/ revascularization model is that it is commonly employed and reproducible. Briefly, the femoral artery of one hind limb is ligated and excised. Laser Doppler perfusion imaging (LDPI) will document any reduction in hind limb blood flow which typically persists for up to seven days in wild-type mice. Hind limb blood flow is progressively augmented over the course of 14 days, typically attaining plateau between 21 and 28 days. Capillary density increases generally will correspond temporally to the blood flow recovery detected by LDPI.

Approach.
Data from group comparisons will provide insights into the role of IL-19 in ischemic neovascularization, and characterization of neovascularization will include four metrics:

1) Arteriogenesis will be defined by the number and volume of arterioles >36 μm
2) Angiogenesis will be defined by number and density of capillaries, defined as vessels <10 μm without α-SMA investment, and by the number of CD36+ angiogenic sprouts.
3) Perfusion will be determined by laser Doppler imaging
4) Vascular remodeling will be characterized using immunohistochemistry with comparisons made between the relative vessel length densities represented by mature, actively remodeling, and immature vessels in each group.

Results.
We have had two setbacks concerning this series of experiments. First, we were not allowed to breed our mice for 5 months because of an MHV virus in our animal facility. This has been resolved, and we resumed breeding in March. Second, our Laser Doppler has been broken, and it has only recently been repaired. As a result, thus far we have examined 7 animals by immunohistochemistry only. However, our data is very promising, as shown in Figure 1, IL-19$^{-/-}$ mice have a reduced capacity to form capillaries post-hindlimb ischemia. As an alternative approach, we have repeated the same experiment with wild-type mice while injecting 10ng/g/day IL-19 during the duration of the experiment. Figure 2 shows in increased capacity to form capillaries in these mice.

In Aim 2 we will determine if mice have a reduced capacity to form microvessels toward IL-19-containing matrigel plugs. These experiments were very successful and have been published (1).

Together, these results suggest that absence of IL-19 impairs angiogenesis, and an increase in IL-19 can exacerbate beneficial angiogenesis. The second aim results indicate that IL-19 is pro-angiogenic and can induce fully formed neovessels with lumens.

1. Jain S, Gabunia K, Kelemen SE, Panetti TS, Autieri MV. The anti-inflammatory cytokine interleukin 19 is expressed by and angiogenic for human endothelial cells. Arterioscler Thromb Vasc Biol. 2011 Jan;31(1):167-75.

Figure 1. Impaired neovascularization in IL-19-/- mice. Gastrocnemius muscles were harvested and processed for immunohistochemistry with anti-CD31 antibody at 28 days post-hindlimb ligation. Expressed as number/mm^2 from all mice from at least 4 mice (P<0.05)

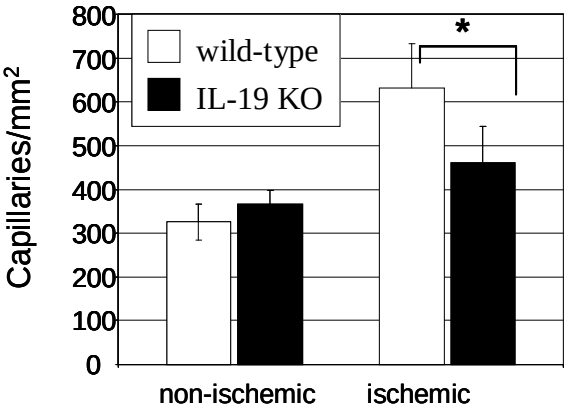

Figure 2. Improved neovascularization in wild-type mice injected with 10ng/g/day IL-19. Gastrocnemius muscles were harvested and processed for immunohistochemistry with anti-CD31 antibody at 28 days post-hindlimb ligation. Expressed as number/mm^2 from all mice from at least 4 mice (P<0.05)

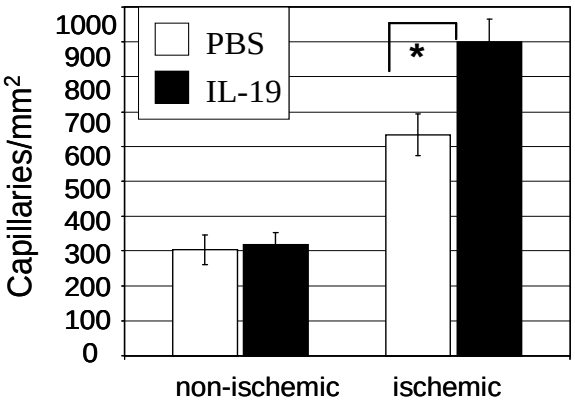

Figure 3. IL-19 stimulates angiogenesis in vivo. C57BL/6 mice were injected sub-cutaneously with Matrigel premixed with PBS control, VEGF, or IL-19. Matrigel plugs were immuno-stained for PECAM1. Positive stained lumens normalized to unit area were quantitated (P<0.05 IL-19 Vs PBS (1)

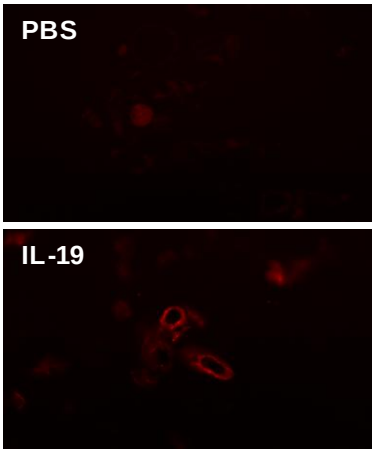

Research Project 3: Project Title and Purpose

A Targeted Drug Delivery System for Preventing Cardiac Remodeling after MI - Cardiac remodeling after myocardial infarction increases the stress on the surviving myocardium and predisposes viable myocardial cells to premature death leading to heart failure. Presence of an appropriate microvasculature is a prerequisite for preventing cardiac remodeling and improving cell survival resulting in maximal regeneration of a functional tissue after myocardial infarction. The goal of this project is to use targeted delivery of pro-angiogenic agents to enhance the morphology and function of post-infarct neovasculature, prior to scar formation, and to establish the optimal time post-myocardial infarction when pro-angiogenic interventional strategies could prevent cardiac remodeling and congestive heart failure.

Duration of Project

7/1/2010 – 6/30/2011

Project Overview

Myocardial infarction (MI) often leads to congestive heart failure (CHF) which is a leading cause of death in the United States and other industrialized countries. Cardiac remodeling after an MI increases the stress on the surviving myocardium and predisposes myocardial cells to premature death. Subsequent tissue repair does not involve a significant regeneration of the supporting microvasculature, which is a key component of the in vivo microenvironment necessary for

survival of cells and the repair after injury and/or the engraftment of a functional engineered tissue. Recent data even suggest that the disappointing attempts at rebuilding the injured cardiac tissues using stem cells may be due to a lack of supporting microvasculature post-MI. However, concerns over possible side effects have hampered attempts at revascularizing the infarcted myocardium using systemic delivery of pro-angiogenic compounds such as *vascular endothelial growth factor* (VEGF) and/or *basic fibroblast growth factor* (bFGF). The goal of this project is to use targeted delivery of pro-angiogenic agents to enhance the morphology and function of post-infarct neovasculature, prior to scar formation, and to establish the optimal time post-myocardial infarction when pro-angiogenic interventional strategies could prevent cardiac remodeling and CHF. We hypothesize that targeted delivery of pro-angiogenic compounds after MI will result in the formation of new vessels in the immediate microenvironment, preventing or moderating cardiac remodeling. The specific aims of this project, using a rat model of MI, are to: 1) Develop immunoliposomes containing pro-angiogenic compounds and determine the mechanisms by which these drug carriers are incorporated into activated endothelium; and 2) In an infarct model in vivo, selectively deliver pro-angiogenic compounds to the infarct region using immunoliposomes, and determine if this targeted delivery approach results in significant improvements in cardiac morphology and function and prevention or moderation of cardiac remodeling. We will also study the efficacy of combining targeted delivery of pro-angiogenic compounds with stem cell therapy to determine if this combinational therapy can significantly improve vascularity, perfusion, and cardiac function when compared to targeted pro-angiogenic therapy alone. Development of this powerful technology will not only significantly prevent cardiac remodeling but will also improve survival and engraftment of engineered tissue.

Principal Investigator

Mohammad F. Kiani, PhD
Professor and Chair
Temple University
Department of Mechanical Engineering
1947 N. 12th Street
Philadelphia, PA 19122

Other Participating Researchers

Rabee Cheheltani, MS, Deborah Crabbe, MD, Ausim Azizi, MD - employed by Temple University

Expected Research Outcomes and Benefits

Expected research outcomes of the project are:

1) Development of immunoliposomes containing pro-angiogenic compounds and determination of the mechanisms by which these drug carriers are incorporated into activated endothelium.
2) Development of a system for selective delivery of pro-angiogenic compounds to the infarct region using immunoliposomes; and a methodology for significantly improving cardiac morphology and function, and preventing or moderating cardiac remodeling.

Pro-angiogenic therapy, especially if administered systemically, has many observed and potential side effects including unintended angiogenesis in distant tissue, increased microvascular permeability, development of new or enhanced growth of existing neoplasms, and increased atherosclerotic plaque mass and instability, among others. However, many of these side effects are circumvented through a targeted drug delivery approach in which the drugs/molecules/genes can be preferentially targeted to the infarct region via the upregulation of various adhesion molecules in the infarct region. Our study will use adjunctive targeted delivery of VEGF and/or bFGF to prevent cardiac remodeling and augment regeneration and myocardial angiogenesis after stem cell implantation.

Summary of Research Completed

Specific Aim 1
Research Design and Experimental Approach: We have developed clinically relevant drug carriers (immunoliposomes) bearing mAbs to adhesion molecules that are upregulated on the vasculature of infarct tissue to show that particles can be targeted to infarct tissue and to optimize particle design and drug loading & release profiles in vitro. Our studies have shown that the type and time course of adhesion molecules on cytokine activated endothelial cells in vitro are similar to cytokine activated endothelium in the infarct tissue. Adhesion assays will be conducted using endothelial cells 5hr, 24hr, 48 hr and 72 hr post in vitro activation. We have also studied the mechanisms by which immunoliposomes bind to and are internalized into activated endothelium in vitro using radiolabeled immunoliposomes. We have started our investigation with drug carriers bearing mAbs to P-selectin due to the fact that this molecule is known to be upregulated post-MI.

Results:
Long circulating liposomes with no antibody had a mean size of 173.2±3.7 nm; the addition of antibody to the surface of liposomes slightly increased their size to 190.6±3.7 nm. The number of antibody molecules attached to the surface of the liposomes were calculated from the size of the liposome and the assumption that, on average a lipid molecule occupies a cross sectional area of 0.7 nm^2. Based on these assumptions each liposome had 16.3±4.1 antibody molecules on its surface. From the data shown in Figure 1, we observe minimal leakage of the VEGF from the immunoliposomes when stored at -80°C over the first 3 weeks of storage. Implementation of this storage technique provides 3 weeks of consistent batch dosing which subsequently reduces any potential error which could result from the differences between the preparations of multiple batches used in multiple experiments. By day 120, we see a 50% loss in VEGF inside the liposomes.

Fluorescent anti-P-selectin immunoliposomes showed a 70-80% preferential adherence to well plates coated with immobilized P-selectin when compared with the adherence of liposomes not conjugated with anti-P-selectin. Some preferential nonspecific binding was also observed in anti-P-selectin immunoliposomes.

Specific Aim 2
Research Design and Experimental Approach: In this study we have assessed the functional significance of pro-angiogenic therapy post-MI in terms of neovascular formation, oxygen

delivery capacity, cardiac function, and cardiac remodeling using in part novel techniques developed in our laboratory. Three experimental groups were investigated: I) no treatment (saline injection), II) targeted pro-angiogenic therapy, and III) systemic pro-angiogenic therapy. These results were then compared with untreated infarct animals in which no pro-angiogenic therapy was present and those obtained with the systemic administration of pro-angiogenic compounds.

We have conducted our studies with large infarcts as measured by echocardiography with the expectation that the remodeling would be first seen in animals with larger infarcts. In our study, a large myocardial infarct was defined as those which have significant left ventricular dilation (left ventricular end diastolic dimensions greater than two standard deviations above the mean), in association with a pattern of restrictive filling (e/a ratio > 2.0) and a reduced deceleration time (less than 50 msec) on pulse wave Doppler. In our experience, these abnormalities correlate with the morphologic and functional abnormalities seen with infarctions of greater than 40% of the LV circumference.

Results

Cardiac functional evaluation using echocardiography showed that targeted drug delivery of VEGF to MI tissue improves cardiac function. For example, as shown in Figure 2, VEGF-IL treatment over 4 weeks resulted in significant improvements in left ventricular end diastolic diameter (Normal (no MI), n=20 animals; Untreated MI, n=4 animals; VEGF-IL Treated MI, n=8 animals; error bars are ± SEM).

At four weeks, hearts were excised and stained with Gomori's trichrome and picrosirius red to quantify collagen deposition and infarct size. As shown in Figure 3, picrosirius red staining indicates that untreated MI hearts exhibit significantly greater collagen deposition compared to targeted VEGF treated heart tissue. Overall, targeted VEGF treated hearts showed a 37% decrease in collagen deposition in the anterior wall, as well as significant improvements in LV filling pressures.

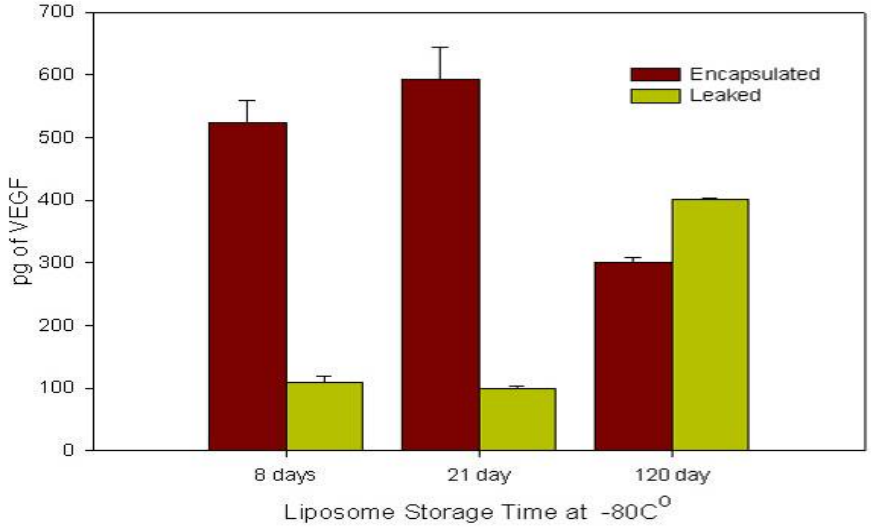

Figure 1

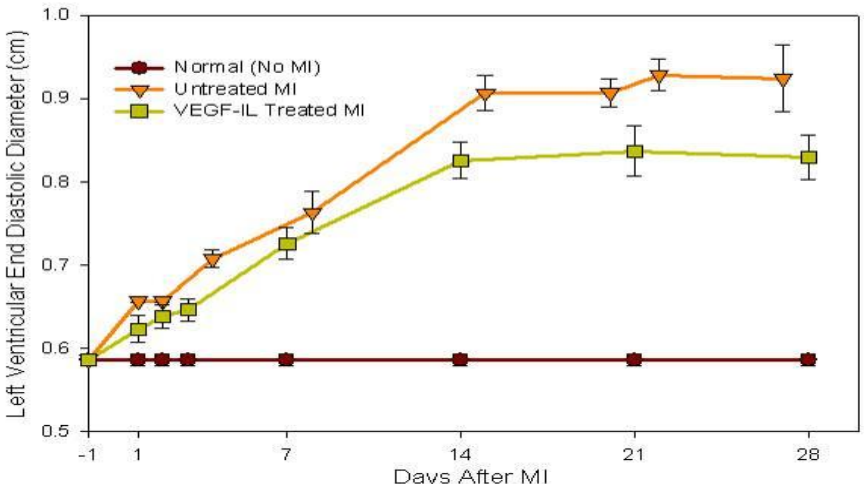

Figure 2

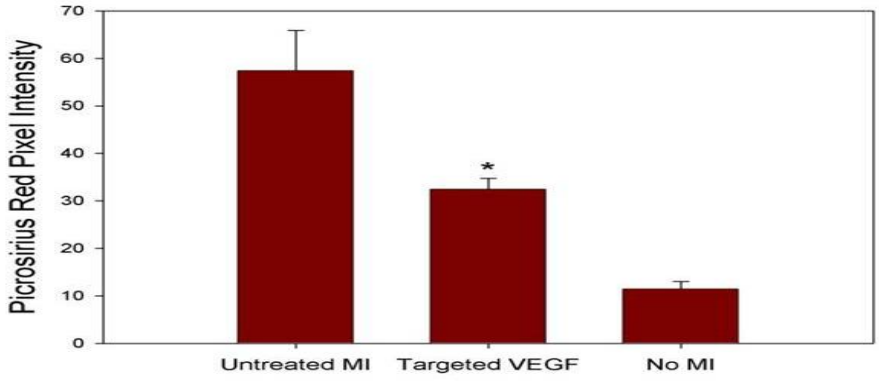

Figure 3

Research Project 4: Project Title and Purpose

Mechanism(s) of Vascular Damage in Obesity - Cardiovascular disease accounts for much of the morbidity and mortality ultimately suffered by patients with diabetes mellitus. Adiponectin is a protein from fat cells that circulates in the bloodstream and has been shown to protect the blood vessels in diabetes. Interestingly, adiponectin opposes the adverse effects on blood vessels of several factors including glucose that is known to be elevated in Type 1 and/or Type 2 diabetes. In this project, we seek to identify the cellular mechanisms by which adiponectin exerts its salutary effects in the endothelial cells that line the blood vessels. These results will advance our understanding of the role of adiponectin in vascular protection in diabetes and in obesity with insulin resistance, conditions with a high risk of life-threatening cardiovascular complications.

Anticipated Duration of Project

9/1/2011 – 8/31/2012

Project Overview

The goal of this project is to define integrative mechanisms by which adiponectin preserves endothelial function in obesity-associated diabetes. The PI reported in the *Journal of Clinical Investigation* in 2007 that adiponectin deficient mice exhibit a distinct inflammatory phenotype in both micro- and macrovascular beds with endothelial dysfunction characterized by impaired endothelial nitric oxide (eNO) generation and increased leukocyte-endothelium interactions due to increased expression of the endothelial cell adhesion molecules (eCAMs), E-selectin and VCAM-1. This inflammatory phenotype was reversed by Ad-replenishing therapy, which was shown to act via enhancing eNO bioavailability, a well-known regulator of eCAMs expression. In metabolic disorders such as obesity and diabetes, loss of physiological eNO levels is in part attributed to eNOS uncoupling by reactive oxygen species (ROS) and it is linked to endothelial dysfunction with inflammatory leukocyte-endothelium interactions. Very recent studies have also suggested that adiponectin reduces accumulation of myeloperoxidase (MPO) in inflamed tissues. MPO is a powerful oxidant released by activated leukocytes that is able to bind to the vascular endothelium where it drastically reduces eNO bioavailability by catalytic consumption. W*e hypothesize that the action of adiponectin to enhance eNO bioavailability and attenuate leukocyte-endothelium interaction in the vasculature largely occurs both via direct suppression of endothelial ROS generation and prevention of leukocyte-derived MPO binding to the endothelium, two novel integrated mechanisms of the vascular protective effects of adiponectin in obesity and diabetes*. Using a genetic mouse model of obesity-associated type II diabetes along with selected knockout mouse technology this project will test the following hypotheses according to these Specific Aims: *1)* To study the effect of adiponectin on eNO/ROS balance and endothelial function *in vivo*; *2)* To study the role of leukocyte-derived MPO in the endothelial protective action of adiponectin.

Summary: The results of these studies will provide important information on the intercellular mechanisms of the anti-inflammatory action of adiponectin in Type II diabetes. They will also provide new insight into the integrative mechanisms by which the endothelium and circulating leukocytes synergize to increase oxidative stress in the obese, diabetic vascular endothelium.

Principal Investigator

Rosario Scalia, MD, PhD
Associate Professor of Physiology
Temple University
3500 N. Broad Street
Medical Education and Research Building 1049
Philadelphia, PA 19140

Other Participating Researchers

Catherine Malkovick, BS - employed by Temple University

Expected Research Outcomes and Benefits

We expect to uncover the mechanisms by which adiponectin protects vascular function. In particular we anticipate finding that reduction of oxidative stress in the mitochondria is one of the key mechanism of the vascular protective action of adiponectin. We will also define the mechanisms by which the various circulating forms of adiponectin exert vasculoprotective effects, with a focus on endothelial cell function *in vivo* using mouse models as well as cultured endothelial cells *in vitro*. Overall, this project will uncover novel mechanisms of vascular damage in obesity and diabetes and it will provide a framework for developing new therapeutic strategies to avert vascular and organ damage in obese, insulin resistant humans.

The developed world is currently experiencing an epidemic of cardiovascular disease that is caused by an ever-increasing prevalence of obesity with insulin resistance due to excess caloric intake and sedentary lifestyles. A key contributor to this increased vascular risk is endothelial dysfunction, a major component of the initiation of the complex process of atherogenesis. By studying the effects of adiponectin isoforms in vascular endothelial cells, we will contribute to our understanding of the mechanisms by which adiponectin exerts its salutary effects on vascular impairment induced by several major agonists that accompany obesity and diabetes. A greater understanding of these signaling pathways may ultimately lead to new targets for the prevention or treatment of the early vascular injury that accompanies obesity and diabetes.

Summary of Research Completed

This project has been delayed and is scheduled to begin 09/01/2011.

Research Project 5: Project Title and Purpose

Targeted Multidrug Delivery System to Overcome Chemoresistance in Breast Cancer – In this project, the Principal Investigators propose to develop a novel multidrug delivery system for the treatment of breast cancer. This novel treatment strategy would provide a significantly more efficacious platform for breast cancer treatment than current treatments.

Anticipated Duration of Project

12/1/2010 – 12/31/2011

Project Overview

Objective/Hypothesis: Our long term goal is to develop a novel combination delivery system that can increase the efficacy of the treatment of the tumor and reduce the toxicity of high-dose systemic chemotherapy. Our objective for this project is to develop and use a combination delivery system to treat breast cancer by targeted liposomal delivery of a combination of intracellular therapeutic drugs (Doxorubicin and verapamil) into the tumor cells to overcome breast cancer chemoresistance, and liposomal delivery of an extracellular therapeutic drug

(bevacizumab) to the interstitial space to inhibit tumor growth. Our hypothesis is that this combination therapy will be superior to single targeted delivery therapies. In the immunoliposomes, the incorporated targeting moieties highly specific to the surface of cancer cells will facilitate the internalization of the combination of an intracellular therapeutic drug and its sensitizer into the tumor cells to overcome drug resistance. The liposomes will deliver an extracellular therapeutic drug to the interstitial space to inhibit the tumor growth by interfering with cell-cell communications. This combination therapy will maintain efficacious systemic drug levels with a better sustained release profile and without added toxicity.

SPECIFIC AIMS:

1. *Synthesize and characterize the liposomes and immunoliposomes:* The liposome will be synthesized and then encapsulated with extracellular therapeutic drug (Bevacizumab). The immunoliposome will be synthesized and conjugated with a targeting moiety (Her-2/neu), and encapsulated with intracellular therapeutic drugs (Doxorubicin and Verapamil).

2. *Evaluate the therapeutic efficacy of the delivery systems in vitro against a breast cancer cell line:* The therapeutic effects of the synthesized delivery systems (liposomes and/or immunoliposomes) will be tested on a Her-2/neu positive breast cancer cell line either individually or in combination. Cellular uptake and intracellular retention will be assessed using fluorescence labeling techniques.

Principal Investigator

Bin Wang, PhD
Assistant Professor, Engineering
Temple University
1947 N. 12th Street
Philadelphia, PA 19122

Other Participating Researchers

Mohan P. Achary – employed by Temple University

Expected Research Outcomes and Benefits

It is our expectation that development of this novel mode of breast cancer therapy will produce a new and exciting therapeutic option. Specific properties of the combination therapy (e.g., blocking a number of pathways rather than a single one) increase the efficacy of tumor treatment. This unique combination delivery system will significantly improve the treatment outcome of breast cancer by increasing treatment efficacy, reducing side effects, and overcoming drug resistance. The successful completion of this project will provide a better alternative for patients in the treatment of breast cancer and ultimately help in eradicating breast cancer mortality. In summary, this research will result in a new treatment for breast cancer that could beneficially impact survival and quality of life for patients with this disease.

Summary of Research Completed

During this study period, a series of experiments have been conducted toward specific aim 1.

1. Preparation of Stealth Liposomes

The first step toward the final goal is to synthesize the liposomes we need. Liposomes that encapsulate Doxorubicin (DOX) & Verapamil will be delivered into the cell, for this purpose, 100 nm liposome will be used as it balances entrapment efficiency (the bigger the size, the higher the entrapment efficiency) and uptake efficiency (smaller size particles are generally easier to enter the cells). For Bevacizumab delivery, 200 nm liposomes are chosen since they will be delivered into the interstitial space of the tumor tissue.

Long circulating liposomes were composed of 50 mole % hydrogenated soy L-α-phosphatidylcholine (HSPC), 45 mole % cholesterol, 3 mole % 1,2-distearoyl-*sn*-glycero-3-phosphoethanolamine-N-[(polyethylene glycol)2000] (DSPE-PEG2000), and 2 mole % DSPE-PEG-maleimide. In our experiment, a total of 40 nano mole lipids were dissolved in chloroform with. After mixing, the lipids were dried under vacuum overnight, and then the lipid film were rehydrated in 40ºC deionized water to form vesicles. The lipids were then extruded 11 times using a thermobarrel extruder. Liposomes at different sizes were achieved by choosing filters with different sizes. Here we used 200, 100 and 80nm size filters respectively. Table 1 summarizes the liposomes size distribution after passing them through different size filters.

Liposome size was measured by dynamic light scattering (DLS) using a Malvern Zetasizer. Size measurements were taken in triplicate at 25°C using a 1:100 (vol/vol) dilution of the liposome suspension in distilled water. The particle size was estimated from cumulant analysis once the correlation was determined. The polydispersity index was used as a measure of particle size distribution, scaled from 0 to 1, where bigger numbers indicate a wider size distribution.

As we can see from the table, the mean diameters of liposomes passing through 100 and 200 nm filters were 113.3 ± 0.6 nm and 192.1 ± 1.3 nm, respectively. Polydispersity index were 0.112 ± 0.012 and 0.047 ± 0.013 for both sizes, respectively. The small polydispersity index indicates a tight size distribution around the mean.

2. Bevacizumab ELISA

In order to be able to determine the Bevacizumab concentration, a direct Enzyme-Linked Immunosorbent Assay (ELISA) method was developed. Briefly, a serial dilution of Bevacizumab solution with known concentration was made using 50 mM carbonate buffer, pH 9.6 (15 mM Na_2CO_3 and 35 mM $NaHCO_3$). 100 µL of Bevacizumab at each concentration was added to an ELISA plate, duplicate. The plate was placed in 4ºC refrigerator overnight to allow for Bevacizumab attachment. Unbound Bevacizumab was then removed with 100 mM pH 9.2 $NaHCO_3$ wash (5 minutes each, on shaker, repeat 3 times). Remaining uncovered plate area was occupied with blocking buffer (3% BSA + 0.1% Tween 20 in HBSS) for 2 hours. Excessive blocking buffer was then removed by 3 times wash with washing buffer (1% BSA + 0.05% Tween 20 in HBSS). After applying anti-human IgG (Fc specific)-peroxidase detection antibody

(1.5 µg/mL, 100 µL/well) for 1.5 hours at room temperature, the plate was ready for color development. After 3 times wash, color develop was archived by adding peroxidase substrate 3.3.5.5′-tetramethylethylenediamine (TMB) to each well and letting it develop at room temperature for 30 minutes. Finally, color development was stopped by adding 50 µl of 1N sulfuric acid to each well. The resulting yellow color can be read at 450 nm in a plate reader.

Figure 1 showed the result of the ELISA assay. This direct Bevacizumab ELISA can test as low as 0.5 µg/mL concentration. Beyond 8 µg/mL concentration, the absorbance value started to saturate and became not linear. Below 8 µg/mL, the ELISA assay showed a good linearity as indicated by the R square value.

3. Bevacizumab Percentage of Entrapment

A dehydration/rehydration method was used to encapsulate Bevacizumab into liposomes. Plain liposome particles were made as described in section 1. Bevacizumab was added to the liposome suspension at a concentration of 250 µg/mL, with a 1:1 volume ratio of Bevacizumab : liposomes. The mixture was first flash froze in dry ice/2-propannol/acetone bath and then lyophilized to powder form. To resuspend the powder, a two step rehydration procedure was employed. First, 0.2 mL of Tris/saline buffer was added to the powder at temperature <40°C; second, lightly rotate/vortex the flask to wet and resuspend the liposomes. Finally, add additional Tris/saline buffer slowly up to 1 mL.

The separation of liposome entrapped Bevacizumab and free Bevacizumab were achieved by centrifugation 1 mL liposome sample at 80,000 *g* for 60 minutes in an ultracentrifuge. After centrifugation, the supernatant was removed and the liposome pellet was resuspend in 1 mL of Tris/saline buffer. To release all the entrapped Bevacizumab, high-frequency ultrasound was used to disrupt the liposomes. The percentage of Bevacizumab entrapment was determined by calculating the ratio of entrapped Bevacizumab to the total amount of Bevacizumab added. According to our calculation, 93.73 nano mole of Bevacizumab were entrapped, since the total amount added was 250 nano mole, the calculated percentage of entrapment was 93.73/250 = 37.5%.

4. Bevacizumab Release Profile

Bevacizumab release profile was obtained by calculating the amount of Bevacizumab remaining in the liposome 1, 2, 3, 4, 5, 6, 24, and 48 hours after the centrifuge. The results were shown in Figure 2. Bevacizumab presented two phases of release from the liposomes. The first phase was the burst release; a burst release of 21.13% was estimated from the curve fitting. This fast phase was due to the release of Bevacizumab that was adsorbed onto the surface during the liposome formulation process. Following burst release, the release was mediated by diffusion from the liposome core and degradation of the liposomes, which is much slower compared to the burst release. The total Bevacizumab released in 48 hours was 55.13%.

The attachment of Her-2/neu targeting moiety to the liposomes had been established in our lab and reported in the proposal for this grant. Therefore, this part is not included in this report. We are also currently synthesizing DOX & Verapamil encapsulated liposomes.

Run	Angle	KCps	ZAve	Poly
1	90	358.2	114	0.098
2	90	358.7	112.8	0.117
3	90	358.7	113.2	0.12
Average		358.6	113.3	0.112
+/-		0.3	0.6	0.012

(a)

Run	Angle	KCps	ZAve	Poly
1	90	214.1	193.6	0.038
2	90	215.4	191.5	0.062
3	90	211.9	191.3	0.042
Average		213.8	192.1	0.047
+/-		1.7	1.3	0.013

(b)

Table 1. Size distribution of liposomes (a) after passing through a 100 nm filter 11 times in a thermobarrel extruder; (b) after passing through a 200 nm filter 11 times in a thermobarrel extruder.

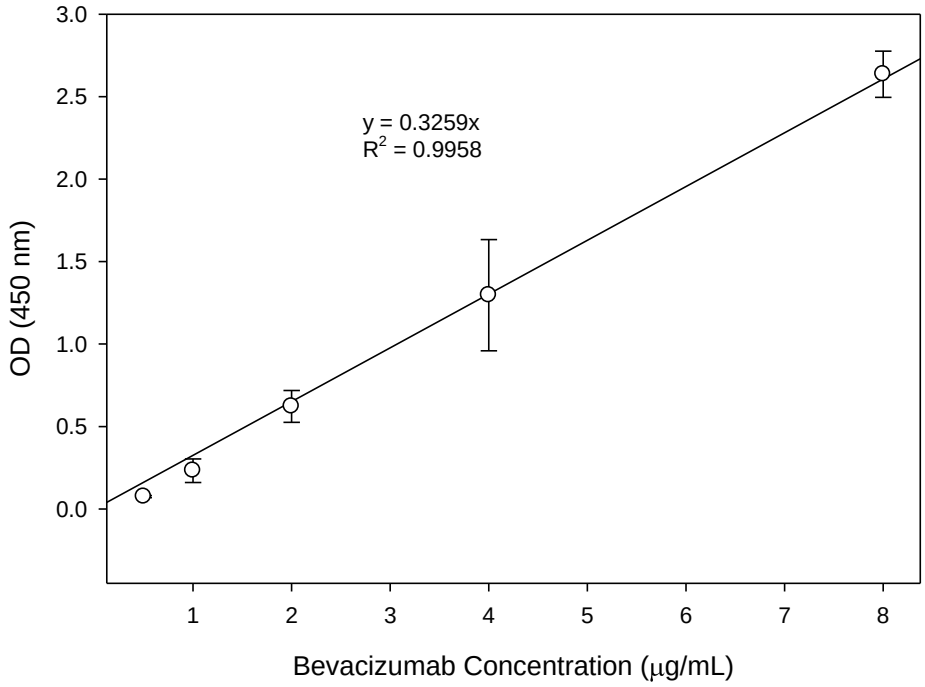

Figure 1. Absorbance value of 0.5, 1, 2, 4, 8 μg/mL Bevacizumab after ELISA assay.

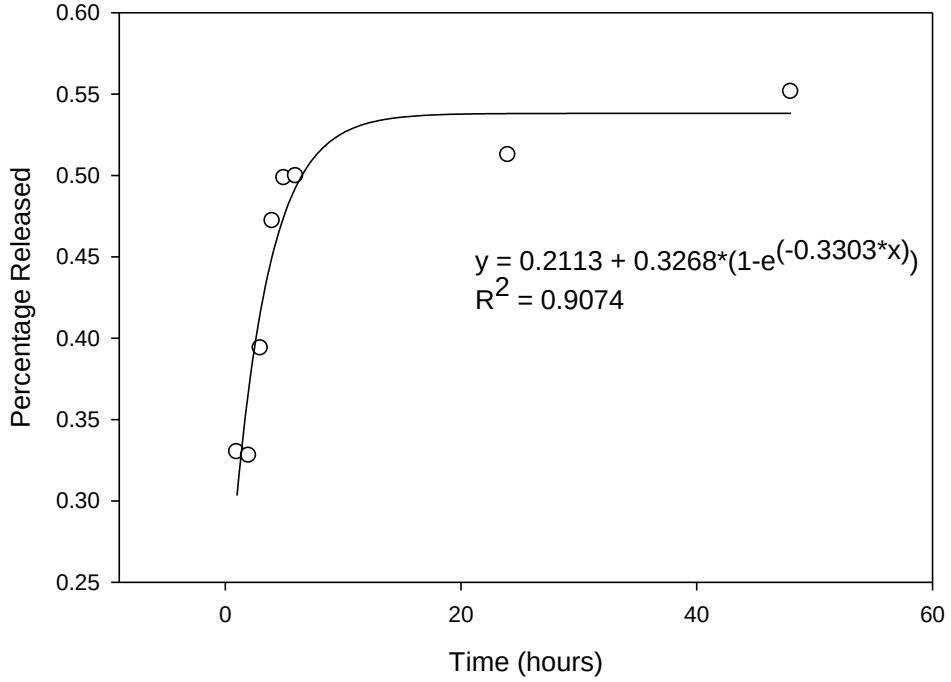

Figure 2. Cumulative Bevacizumab release during 48 hours.

<u>Research Project 6: Project Title and Purpose</u>

Nanoconjugates for Targeted Treatment of Acute Lung Injury – The development of the acute respiratory distress syndrome (ARDS) following infection or injury is a major public health problem and one of the leading causes of death in Intensive Care Units (ICU). ARDS is characterized by excessive neutrophil infiltration of the lungs and neutrophil-mediated lung tissue damage. To date, there are no specific pharmacologic therapies available that protect the lung from neutrophil-mediated damage. We identified the enzyme delta-Protein Kinase C (δ-PKC) as a critical regulator of the inflammatory response. The goal of this project is to develop a specific δ-PKC peptide inhibitor into a viable therapeutic by the use of nanocarriers to transport the inhibitor directly to the lung. If successful, this approach could significantly decrease the morbidity and mortality associated with sepsis, burns, hemorrhagic shock and trauma.

Anticipated Duration of Project

12/1/2010 – 6/30/2012

Project Overview

Acute respiratory distress syndrome (ARDS) is a major public health problem and a leading cause of death in intensive care units (ICU) (>200,000 cases/year). ARDS is characterized by an intense inflammatory response leading to neutrophil infiltration of the lungs and severe lung tissue damage. Treatment of ARDS is largely supportive and no specific pharmacologic

therapies are available that protect the lung from neutrophil-mediated damage. We have identified the Protein Kinase C isotype-delta (δ-PKC) as a critical regulator of the inflammatory response controlling recruitment and activation of neutrophils in the lungs. Delivery of a δ-PKC TAT peptide inhibitor directly into the lungs of a rat model of ARDS had a dramatic anti-inflammatory and lung protective effect indicating this δ-PKC TAT peptide would offer a novel treatment option for ARDS. We have a proven δ-PKC peptide inhibitor which through linkage to a TAT peptide is taken up intracellularly to inhibit δ-PKC activity. To develop this δ-PKC TAT inhibitor into a viable therapeutic, a noninvasive mechanism for drug delivery is needed which selectively targets our δ-PKC inhibitor to the lung. We propose to use nanocarriers to transport our inhibitor directly to the lung. This nanoconjugate will optimize drug delivery, avoid immune cell activation, and protect the therapeutic from proteolytic degradation. Directed delivery of this highly specific δ-PKC-TAT inhibitor to the lungs would offer a protective treatment and could be administered in the emergency room or upon admittance to an ICU.

Aim 1: "Proof-of-concept" experiments to develop a series of nanoconjugate compounds which deliver the δ-PKC TAT inhibitory peptide directly to the lungs. Candidate nanoconjugate compounds will be screened using an in vitro model system of human cells. We will determine the effect of these drug delivery systems on δ-PKC inhibitor binding, intracellular uptake, inhibition of δ-PKC, and effect on neutrophil transmigration.

Aim 2: In vivo testing of radiolabeled (Tc-99m) candidate nanoconjugate compounds to determine uptake and biodistribution in our rodent model of ARDS. These studies will determine effectiveness of the drug delivery system in vivo and the concentration required to inhibit δ-PKC activity in the rat lung.

Principal Investigator

Laurie E. Kilpatrick, PhD
Associate Professor of Physiology
Temple University
Rm 206 PAH Building
3307 North Broad Street
Philadelphia, PA 19140

Other Participating Researchers

Linda Knight, PhD, Steven Kelsen, MD – employed by Temple University

Expected Research Outcomes and Benefits

Targeting δ-PKC offers a novel therapeutic strategy and this δ-PKC TAT inhibitory peptide represents a new class of drugs. To our knowledge, no studies have examined the effects of δ-PKC inhibition as a therapeutic approach to the treatment of ARDS, nor has this inhibitory peptide been coupled to nanocarriers. We have taken a unique approach to this clinical problem by targeted delivery of the δ-PKC-TAT inhibitory peptide to the lung to prevent neutrophil-mediated lung injury. There is a lag time between non-pulmonary injury and the influx of

neutrophils into the lung and the initiation of lung damage. This lag period of between 6-48 hrs, depending on type of injury and severity of injury, offers a therapeutic window where treatment could be initiated that would stop the progression to neutrophil-mediated lung injury. Directed delivery of this highly specific δ-PKC-TAT inhibitor to the lungs would offer a protective treatment and could be administered in the emergency room or upon admittance to an ICU. A significant competitive advantage of our technology is that the δ-PKC TAT peptide is safely tolerated in patients. This peptide inhibitor is currently being tested as a therapeutic for the treatment of acute myocardial infarction. A phase I/II clinical trial to test safety and efficacy was successfully completed and no adverse events were reported following intra-coronary administration of the δ-PKC-TAT peptide for the treatment of acute myocardial infarction (www.kaipharma.com). If our preclinical studies show that the δ-PKC-TAT inhibitor is an effective modulator of neutrophil-mediated lung injury, then it could move rapidly to clinical trials. Far reaching therapeutic applications include acute lung injury, adult respiratory distress syndrome, acute trauma, asthma, interstitial lung disease, emphysema, chronic bronchitis, cystic fibrosis, extracorporeal membrane oxygenation, exposure to irritant gasses, thermal injury, smoke inhalation, SARS, anthrax, radiation exposure, chemicals or toxic substances, and infection.

Summary of Research Completed

Aim 1: "Proof-of-concept" experiments to develop a series of compounds which deliver the δ-PKC TAT inhibitory peptide directly to the lungs. Candidate compounds will be screened using an in vitro model system of pulmonary microvascular endothelial cells.

The objectives of these in vitro experiments are: 1) to load δ-PKC-TAT peptide into carriers, 2) stable loading of the peptide, and 3) intracellular delivery of the δ-PKC-TAT peptide into PMVEC.

Carrier design

To target the pulmonary endothelium we designed carriers composed of multiple components that included an inhibitory δ-PKC peptide and a cell permeable TAT peptide that facilitates intracellular uptake into cell cytosol. The δ-PKC inhibitory peptide was composed of the following aa sequence: SFNSYELGSL. The δ-PKC inhibitory peptide was coupled via an N-terminal Cys-Cys bond to a membrane permeant peptide in the HIV TAT gene product (YGRKKRRQRRR). The use of a disulfide bond limits directed intracellular delivery of the δ-PKC TAT inhibitor to the cytoplasm. We had some of the peptide synthesized with a fluorescent tag at a noncritical site of the δ-PKC peptide, to enable tracking in vitro (5-carboxyfluorescein (5FAM-green label) or hydrazinonicotinate for ^{99m}Tc radiolabeling). *The remaining components of the formulation are not provided pending publication.*

We successfully loaded the 99mTc-labeled δ-PKC TAT inhibitory peptide into Carrier X. The level of peptide loading into the carrier was determined by measuring the peptide after size-exclusion chromatography. Using this method, we obtained a loading efficiency of 40-45% of 99mTc-HyNic-δPKC-TAT. The stability of the complex was determined by measuring the release of the 99mTc-HyNic-δPKC-TAT peptide from the carrier. The complex was suspended in fresh buffer and incubated at 37°C in a Float-A-Lyzer dialysis unit with appropriate molecular

weight cutoff. At select time points over 24 hrs, dialysis buffer was sampled and the release of δ-PKC-TAT peptide from the complex was determined by monitoring radioactivity to determine free peptide in solution as a fraction of the total. The formulation containing the δ-PKC-TAT peptide was stable and showed low levels of δ-PKC-TAT peptide release over 24 hrs of 37°C dialysis as compared to free δ-PKC-TAT peptide (Figure 1).

Drug carrier - pulmonary endothelial interaction was first tested in vitro using human and rat pulmonary microvascular endothelial cells. Human pulmonary microvascular endothelial cells (PMVEC) were purchased from Lonza (Walkersville, MD) and cultured in flasks using endothelial growth medium 2 (Lonza) with added bovine brain extract, vascular endothelial growth factor, epidermal growth factor, gentamycin, and hydrocortisone according to the manufacturer's specifications. Cells were obtained at passage 5 and used between passages 5 and 8. Cells were passed from T-25 flasks into experimental plates when 70–80% confluent and cultured in 96-well plates. Medium was changed on the monolayer every 48 hr. Rat pulmonary microvascular endothelial cells (PMVEC) (VEC Technology, Inc., Rensselaer, NY) were also obtained, cultured to 70-80% confluency and then plated in fibronectin-coated 96 well plates. For binding experiments, rhodamine-tagged drug carriers were added to PMVEC monolayers and incubated for 1 hr at 37°C. The cell monolayers were washed and fluorescence measured using a fluorescent microplate reader. *The results of these experiments are not provided pending publication.*

Carrier uptake into PMVEC

Incorporation of the δ-PKC TAT peptide inhibitor into Carrier X may alter the kinetics of peptide uptake by PMVEC, intracellular targeting, and inhibitory activity. In this series of experiments we examined the uptake and internalization of the formulation with loaded δ-PKC TAT peptide. As shown in Figure 2, a fluorescently tagged δ-PKC TAT inhibitory peptide was incorporated into the drug formulation which was subsequently added to PMVEC and incubated for 20 min at 37°C, washed, and the δ-PKC inhibitory peptide binding to PMVEC was determined by fluorescence microscopy. These studies demonstrated δ-PKC peptide uptake. The effectiveness of delivery of the inhibitory peptide was next evaluated by determining the effect of the formulation on VCAM-1 expression in PMVEC.

Effect of δ-PKC TAT inhibitory peptide on VCAM-1 expression in PMVEC

The goal of this experiment was to test the hypothesis that complexed δ-PKC TAT peptide will be as effective as free peptide in modulating cytokine-mediated activation of pulmonary endothelial in vitro. We determined the effect of the peptide formulation on cytokine-mediated expression of the adhesion molecule VCAM-1 on the surface of PMVEC. The surface expression of VCAM-1 was determined by a cell surface ELISA. PMVEC were grown to confluence in 96-well plates and then pretreated with buffer, free PKC-δ TAT peptide inhibitor (0.01-5 uM) or Carrier X with incorporated δ-PKC TAT (0.1uM-2 uM) for 1hr prior to the addition of IL-1 (10U/ml). The cells were incubated for 18 hrs, washed twice in washing buffer consisting of PBS with 0.5% BSA, 1mM $CaCl_2$ and 1mM $MgCl_2$, and then fixed for 15min at RT in 1% paraformaldehyde. The cell monolayers were washed and blocked for 1hr at 37°C in blocking buffer (washing buffer plus 2% BSA). The cells were incubated with anti-human VCAM-1 (0.25ug/ml, clone 51-10C9, BD Pharmingen) for 1hr, washed, and incubated with goat anti-mouse IgG conjugated to HRP (1:1000) for 1hr. The cell monolayers were washed,

Tetramethylbenzidine (TMB) liquid substrate (Sigma-Aldrich) was added, and optical density (OD_{650}) determined. Mouse IgG1 was used as an isotype control at a concentration of 0.25ug/ml. The value obtained with mouse IgG1 was subtracted from the value obtained for VCAM-1 expression. We found that there was little VCAM-1 expression on PMVEC monolayers under basal or resting conditions. IL-1 stimulated a significant increase in VCAM-1 which was attenuated in a dose-dependent manner by incubation with either free δ-PKC TAT peptide inhibitor or by Carrier X with incorporated δ-PKC TAT peptide (Figures 3 and 4). Thus, δ-PKC selectively regulates activation of PMVEC and IL-1-induced cell surface expression of VCAM-1. Furthermore, these studies indicate that the δ-PKC TAT peptide is still an effective inhibitor when delivered to the endothelium in our test formulation.

Aim 2: To test radiolabeled (Tc-99m) candidate formulations to determine in vivo uptake and biodistribution in rats.

Adult Sprague Dawley rats (225-250 gm) were anesthetized with isoflurane and injected intravenously (tail vein) with radioactive tracer coupled to free δ-PKC-TAT, test formulations and controls in 0.1-0.5 ml volumes. The animals were maintained under anesthesia for 1 hr and imaged by gamma counter at 15 min intervals. At 1 hr post injection, animals were euthanized, and tissue and blood samples collected (Temple Univ. Approved ACUP #3300). Radioactivity was monitored in blood, lung, heart, liver, kidney, spleen, muscle and fat tissue. The radioactivity in each tissue was counted in comparison with a standard of the administered dose in order to determine the percent of the administered dose per organ and per gram of tissue. Intravenous administration of the free radiolabeled δ-PKC-TAT peptide resulted in rapid excretion and peptide was found principally in the kidneys, liver and bladder with little localization to lung tissue (Table I) indicating that delivery of the δ-PKC-TAT peptide alone to the lungs is inefficient. We next determined whether our formulation targets the lungs when injected IV. In these experiments, Carrier X was labeled with Tc-99m via the HyNic linker and injected IV into the tail vein of the anesthetized rat. Gamma images were acquired immediately following injection. As shown in Figure 5, there was significant delivery of drug carrier to the lungs. These data indicate that it is feasible to deliver δ-PKC-TAT to the lung with our carrier. *Note: Specific experiments testing in vivo delivery of various components of the carrier are not presented pending publication.*

Figure 1: Release of the δ-PKC TAT Peptide from Carrier X

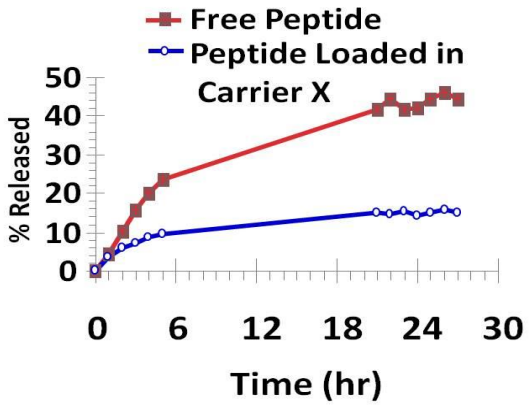

^{99m}Tc-δ-PKC-TAT peptide (free or loaded in Carrier X was dialyzed (20 kDa MWCO) against pH 7.2 buffer at 37°C. Samples (1 ml) of dialysate were counted.

Figure 2: Binding of FAM-tagged δ-PKC peptide loaded in Carrier X to PMVEC

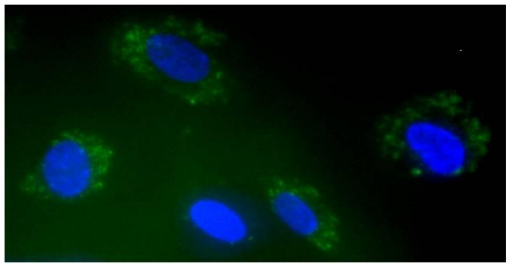

FAM (green)-tagged δ-PKC TAT inhibitory peptide loaded in Carrier X was incubated with rat PMVEC monolayers in chamber slides for 20 min at 37°C. The slides were washed and mounted in Vectashield with DAPI (blue) and imaged by fluorescence microscopy.

Figure 3: Effect of free δ-PKC TAT on VCAM-1 Expression in PMVEC

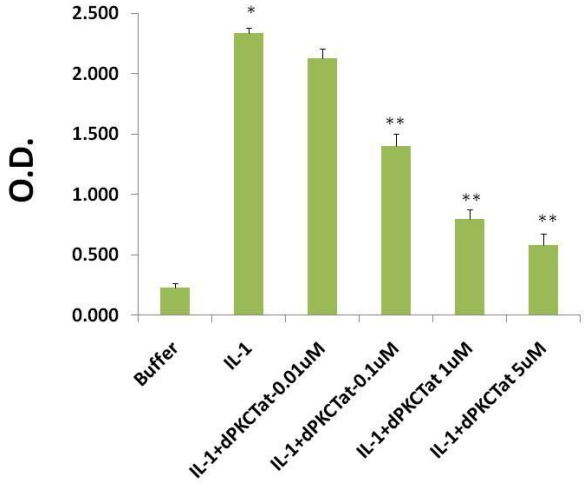

PMVEC were treated overnight with buffer or IL-1±δ-PKC TAT peptide (0.01-5uM). VCAM-1 expression in PMVEC monolayers was determined by ELISA (N=4) *p<0.01 buffer vs. IL-1, **p<0.01 IL-1 vs. IL-1+ δ-PKC TAT (0.1-5uM)

Figure 4: Effect of δ-PKC TAT loaded in Carrier X on VCAM-1 Expression in PMVEC

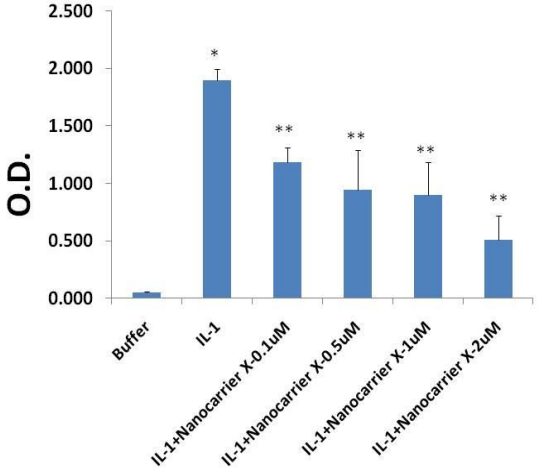

PMVEC were treated overnight with buffer or IL-1±δ-PKC TAT peptide loaded in Carrier X (0.1-2uM). VCAM-1 expression in PMVEC monolayers was determined by ELISA (N=4) *p<0.01 buffer vs. IL-1, **p<0.05 IL-1 vs. Carrier X (0.1-2uM)

TABLE I	
	Tc-99m-δPKC-TAT peptide
	%ID/g
blood	0.36
heart	0.16
lungs	0.50
spleen	0.63
liver	1.69
kidneys	3.14
muscle	0.05
fat	0.03

Labeled peptide was administered IV (tail vein) to normal rats. After 1 hr, animals were euthanized. Tissue and blood samples were removed for weighing and counting for Tc-99m. Counts were compared with a standard of the administered dose.

Figure 5: Tissue Distribution of Carrier X

Uptake of (^{99m}Tc) labeled Carrier X immediately following IV injection in the tail vein of normal rats. Uptake was observed primarily in the lung, liver and kidneys.

Research Project 7: Project Title and Purpose

Role of Dorsostriatal Glutamatergic Signaling in the Regulation of Cocaine-induced Synaptic and Behavioral Plasticity – Chronic drug use leading to drug addiction is associated with impairments in reinforcement seeking behaviors. The pathological mechanisms associated with these maladaptive behaviors are not known. The primary goal of this project is to understand the role of dorsostriatal glutamatergic signaling in the regulation of drug (cocaine)-induced synaptic plasticity and behavioral sensitization. To accomplish this goal, we will utilize multidisciplinary approaches in neurosciences to gain an integrative perspective on the neurobiological basis of compulsive cocaine-seeking behaviors. Results from this project will provide important preclinical data on potential targets for treatment of cocaine addiction.

Anticipated Duration of Project

12/1/2010 – 12/31/2011

Project Overview

Deficits in cognitive control play an important role in the representation of compulsive drug-taking and seeking behaviors. Recent evidence suggests that diminished ability to control drug seeking arise from perturbations in glutamate homeostasis that produces impairments in prefrontal regulation of striatal circuitry. Specific corticostriatal circuits involving discrete

regions of the dorsal striatum contribute directly to the manifestation of executive functions through the integration of sensorimotor, cognitive and motivational information. Specifically, components of medial and lateral dorsostriatal structures are essential for learned associations to become habitual, and abnormal activity within these loops is implicated in compulsive drug seeking. However, mechanisms underlying the drug-induced neuroadaptations in glutamate homeostasis in dorsal striatal structures and their role in enduring drug use and relapse, and executive dysfunction are not known.

In this project we will determine the effects of acute and chronic cocaine administration on the spatiotemporal dynamics of glutamatergic transmission in the dorsomedial and dorsolateral striatum in rats. We will utilize enzyme-based biosensors and electrochemical recordings approaches to measure glutamatergic activity in *real time* in *awake freely-moving* animals. The effect of ceftriaxone, a beta-lactam antibiotic known to upregulate the expression and functional activity of glial glutamate transporter (GLT1), will also be examined on striatal glutamate homeostasis in chronic cocaine-treated animals. As striatal dopamine mediates the reinforcing effects of drugs and also regulates glutamate release, we will also elucidate the involvement of dopaminergic mechanisms in cocaine-induced changes in striatal glutamatergic activity. Finally, we will study the effects of pharmacological manipulations that disrupt signaling via iGluRs and mGluRs on the acquisition and expression of cocaine-induced locomotor sensitization, and cognitive flexibility.

Principal Investigator

Vinay Parikh, PhD
Assistant Professor
Temple University
Department of Psychology
1701 N. 13th Street, Weiss Hall
Philadelphia, PA 19122

Other Participating Researchers

Ellen M. Unterwald, PhD, Scott M Rawls, PhD – employed by Temple University

Expected Research Outcomes and Benefits

We anticipate that repeated but not acute cocaine administration will result in neuroadaptations in the glutamatergic synapses in the dorsal striatum. These plastic changes in the dorsostriatal glutamatergic circuits will be dependent on intact dopaminergic innervation of the striatum. Furthermore, we hypothesize that ceftriaxone, a glial glutamate transporter 1 activator, will be able to prevent the cocaine-induced changes in glutamatergic neurotransmission while dampening the behavioral effects of repeated cocaine due to its effects on this transporter. Finally, we expect that the striatal administration of ionotropic glutamate receptor antagonists will attenuate behavioral sensitization associated with chronic cocaine administration. The expected results will form the basis of future research to explore neurobiological mechanisms that regulate synaptic plasticity in the dorsal striatum and contribute to the habitual use of

cocaine, subsequently leading to compulsive cocaine seeking and addiction. Furthermore, these studies will identify biological targets that recruit brain circuits triggering compulsive cocaine seeking to be exploited for development of therapeutic strategies for not only cocaine, but in general, drug abuse and addiction.

Summary of Research Completed

We have made enormous progress during the first six months of the funding with respect to aims 1 & 3 of the proposal. We conducted an extensive series of experiments that utilized a combination of neurochemical and behavioral neuroscience approaches to determine the contribution of glutamatergic signaling to chronic cocaine-induced plasticity in dorsolateral(DL)-striatum and behavioral sensitization.

Chronic cocaine treatment and striatal glutamate dynamics (Aim 1)

Male Wistar rats received either saline or cocaine (20mg/Kg/day; i.p.) for two weeks. During the subsequent abstinence phase (5-7 days), animals were prepared for electrochemical recordings of glutamatergic transmission. Enzyme-based biosensors were employed to monitor the dynamics of resting (basal) and depolarization-evoked glutamate release from the DL-striatum of *awake* freely-moving animals following saline or cocaine challenge. Raw traces of glutamate signals from a control (saline pretreated/saline challenged; SAL/SAL) and drug (cocaine pretreated/cocaine challenged; COC/COC) treated animal following local infusions of potassium (KCl 70mM; 1 µL) are shown (Fig. 1). Cocaine challenge slightly increased the amplitudes of potassium-evoked signals in cocaine-pretreated animals (9.52 ± 4.82 µM vs. 6.32 ± 0.99 µM in controls). Furthermore, the clearance of depolarization-evoked glutamate release, expressed as time required to reduce the peak signal amplitude by 50% (T50), was robustly delayed in cocaine-challenged animals (69±5 s vs. 19±4 s in controls; Fig. 2). Intra-striatal infusion of TFB-TBOA (a non-specific glial transporter blocker) increased resting glutamate levels in saline-treated animals (4.22 ± 0.58 µM above baseline). This increase was lower in cocaine-pretreated animals (1.68 ± 0.56 µm) suggestive of higher baseline glutamate in these subjects. Ceftriaxone (CTX), a beta lactam antibiotic known to activate astrocytic glutamate transporter subtype 1 (GLT-1), attenuated the effects of chronic cocaine on glutamate clearance kinetics. These preliminary data suggest that chronic cocaine treatment increases resting glutamate levels in DL-striatum presumably by downregulating GLT-1.

Ceftriaxone treatment and glial glutamate transporters (Aim 1)

CTX administered repeatedly elicits a modest increase in GLT-1 transporter expression in drug-naïve rats. Data up to this point suggest that the effect spans multiple brain regions in the mesocorticolimbic and are most robust in the dorsal striatum. Present data suggest that GLT-1 expression is not significantly altered in animals that are exposed repeatedly to cocaine (5 or 15 days), withdrawn from cocaine, and then reintroduced to cocaine following abstinence from the drug. On the basis of data suggesting that extracellular glutamate depletion in the NAcc is most profound during later stages of cocaine abstinence (*i.e.*, 3 weeks following discontinuation of cocaine exposure), additional studies are planned to determine if significant changes in GLT-1 transporter expression in the PFC, NAcc, and dorsal striatum are also detectable at this stage. It

is possible that changes in the compartmentalization of GLT-1 transporters, an effect which would not detectable by our current methodological approach, occur during cocaine exposure. For example, cocaine may induce trafficking of GLT-1 transporters between the cytosol and plasma membrane, and CTX may alter this trafficking. Thus, additional studies will test this hypothesis as well as changes in the function of related glutamate transporters such as GLAST (glutamate aspartate transporter) and cysteine-glutamate antiporters.

Potential effects of GLT-1 transporter activation include effects on learning and memory. Behavioral studies using an autoshaping model were conducted to test the effects of chronic administration of CTX on these endpoints. The autoshaping model is a two day procedure which measures whether a drug will affect acquisition, consolidation, or retention of a novel learned response objectively and rapidly. Our findings, presented in Fig. 5, suggest that repeated CTX treatment produces limited effects on learning and memory in male mice in the autoshaping procedure. Related behavioral studies from our laboratory indicate that CTX displays efficacy in a mouse model of self-administration designed to investigate the motivational and reinforcing properties of cocaine.

Striatal AMPA receptors and behavioral plasticity following chronic cocaine (Aim 3)

In a separate series of experiments, the role of dorso-striatal AMPA (α-amino-3-hydroxy-5-methyl-4-isoxazolepropionic acid) glutamate receptors in cocaine-induced behavioral plasticity was explored. CNQX, an AMPA receptor antagonist, or vehicle was infused bilaterally (0.3ug/0.5ul/side) 15 minutes prior to daily injection of cocaine (20 mg/kg, i.p.) or saline in adult male Wistar rats. After 5 consecutive days of treatment, cocaine was withdrawn for 6 days, following which a challenge injection of cocaine (20 mg/kg, i.p.) was given. Locomotor and stereotypical behavior was measured for one hour after each cocaine injection. Results demonstrated that pretreatment with CNQX significantly attenuated the hyperactivity produced by cocaine on each of the 5 days of injection. In addition, CNQX prior to daily cocaine administration blocked the development of locomotor sensitization as tested after the cocaine challenge (Fig. 6). These results indicate that ionotropic glutamate receptors in the dorsolateral striatum are involved in the development of behavioral sensitization to repeated administration of cocaine.

Plans for remaining funding period.

1. To successfully complete all the experiments of Aims 1 & 3 which are currently in progress.
2. To determine the contribution of TTX-sensitive (neuronal) component of resting glutamate during abstinence and drug-challenge phase.
3. To test the hypothesis that attenuation of the effects of CTX on glutamate kinetics in DL-striatum in chronic-cocaine treated animals involve normalization of a downregulated GLT1 expression.
4. To study the effect of chronic cocaine on striatal glutamatergic activity in 6-OHDA lesioned animals (Aim 2).

Significance.

Deficits in cognitive control play an important role in the representation of compulsive drug-taking and seeking behaviors. Specific corticostriatal circuits involving discrete regions of dorsal striatum are essential for learned associations to become habitual, and abnormal activity within these subcircuits is implicated in compulsive drug seeking. However, neurochemical mechanisms underlying the drug-induced neuroadaptations in dorso-striatal structures and their role in enduring drug use and relapse, and executive dysfunction are not known. The proposed experiments will test the hypothesis that chronic cocaine treatment produces neuroadaptive changes in DL-striatum by upregulating resting glutamate levels, and consequent overactivation of ionotropic glutamate receptors is responsible for behavioral sensitization associated with chronic drug use. The expected results will form the basis of future research to explore neurobiological mechanisms that regulate synaptic plasticity in the dorsal striatum and contribute to the habitual use of drugs subsequently leading to compulsive drug use and addiction. Furthermore, these studies will identify biological targets that recruit brain circuits triggering compulsive drug seeking to be exploited for development of therapeutic strategies for drug addiction.

Conference Presentations/Publications

1) Naughton SX, Shi X, Kelley LK, Rawls SM, Unterwald EM, Parikh V. Glutamatergic contributions to cocaine-induced neuroadaptations in dorsolateral striatum and behavioral sensitization. **Society for Neuroscience Abstracts** 2011; 41:99.

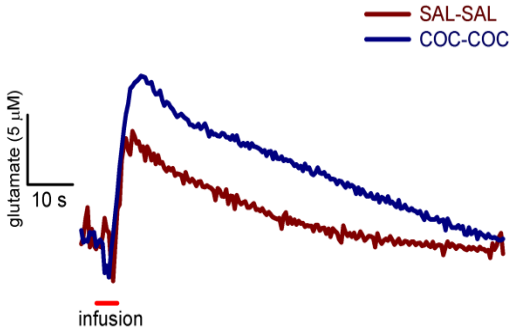

Figure 1. Real-time changes in depolarization-evoked glutamate release in the dorsal striatum of vehicle/drug-treated awake rats.

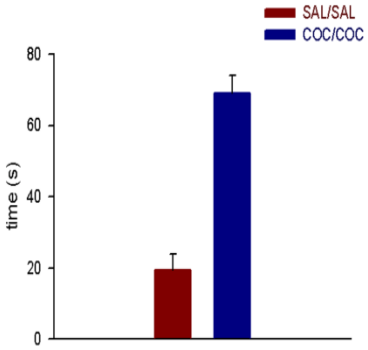

Figure 2. Clearance rate (T50) of potassium-evoked glutamate signals.

Fig. 3

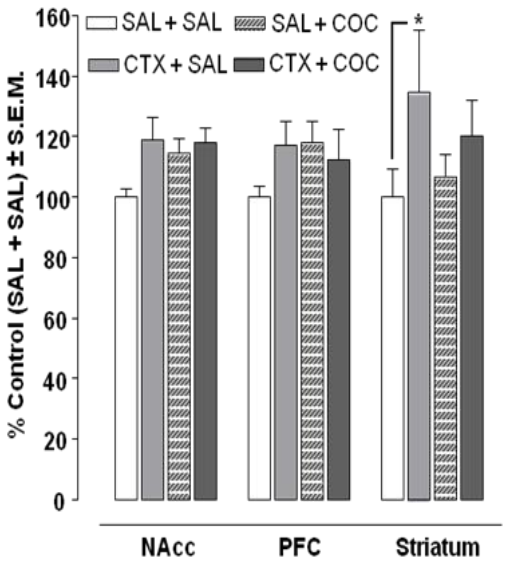

Fig. 3 Effects of CTX and short-term (5 days) cocaine exposure on GLT-1 transporter protein expression in the nucleus accumbens (NAcc), prefrontal cortex (PFC), and dorsal striatum of rats. Rats were injected with CTX (200 mg/kg, ip) or saline once daily for 8 days. Beginning on the fourth day, rats from both groups were injected with cocaine (10 mg/kg, ip) or saline for 5 days. All rats were then withdrawn from drug exposure for 10 days and challenged with cocaine (10 mg/kg, ip). Rats were euthanized 180 min following cocaine challenge and brains were extracted for dot-blot analysis to quantify GLT-1 protein levels. Data are expressed as percentage of the drug-naïve control group (SAL + SAL) ± S.E.M. N = 8 rats per group. Two-way ANOVA (treatment, brain region) indicated a significant treatment effect [F (3, 28) = 3.183, P = 0.0285] but not a significant brain region effect [F (2, 77) = 0.1393, P = 0.0285] or interaction [F (6, 77) = 3.183, P = 0.4573]. *P < 0.05 compared to respective SAL + SAL group (Bonferroni test).

Fig. 4

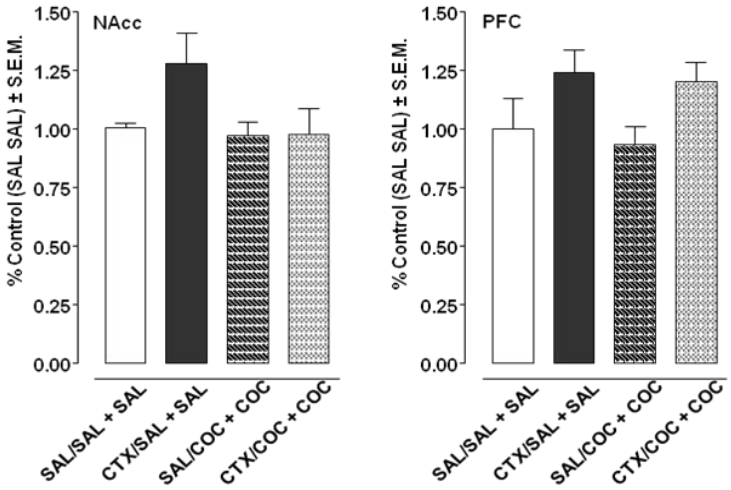

Fig. 4 Effects of CTX and long-term cocaine exposure (2 weeks) on GLT-1 transporter protein expression in the nucleus accumbens (NAcc) and prefrontal cortex (PFC) of mice. All mice received a 3-day pretreatment of CTX (200 mg/kg, ip once daily) or saline prior to the start of cocaine administration. After pretreatment, CTX or saline was concurrently administered (once daily) to rats injected with cocaine (15 mg/kg, ip) or saline for 14-15 days. Mice were then withdrawn from drug treatment for 48 hours prior to receiving an injection of cocaine or saline. Animals were euthanized 120 min later and brains were extracted for Western blot analysis. PFC and NAcc were dissected and gels were loaded 20 ug per lane, transferred to nitrocellulose membrane, and probed with GLT1 (Millipore, guinea pig, 1:20,000 in 2%milk/TBST for 1.5hrs, room temp) and GAPDH (Santa Cruz, mouse, 1:2,000 in 1XTBST for 1.5hrs, room temp). Secondary antibodies were donkey-anti-guinea pig (1:10,000 in 5%milk/TBST for 50minutes, room temp) and goat-anti-mouse (1:5,000 in 1XTBST for 50minutes, room temp). Data are expressed as percentage of the drug-naive control group (SAL + SAL) ± S.E.M. N = 5-6 rats per group. **NAcc)** GLT-1 expression was upregulated in mice receiving CTX pretreatment, but a significant main effect was not identified by one-way ANOVA conducted on the entire data set [F (3, 18) = 2.704, P = 0.0761]. **PFC)** A significant main effect was not identified by one-way ANOVA conducted [F (3, 19) = 2.260, P = 0.1144].

Fig. 5

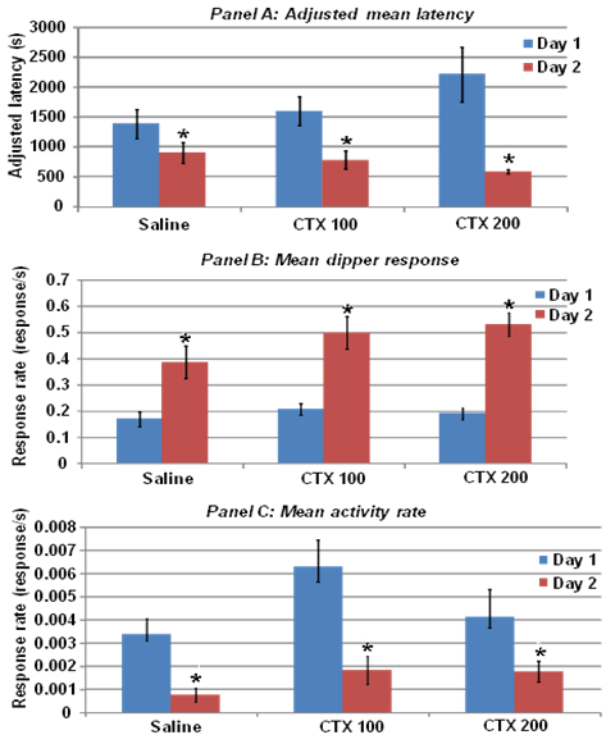

Panel A. **Although 10 days of 200 mg/kg ceftriaxone administration dose-dependently delayed the acquisition of the autoshaped response, the mice still learned and retained the response on Day 2.** All groups of mice earned 10 reinforcers significantly faster on Day 2 than Day 1 (*, $p < 0.05$) indicating consolidation and retention had occurred. However there were not significant differences between the groups as determined by one-way ANOVA on Day 1 or Day 2. Ordinate: Mean adjusted latency was calculated as the amount of time from the 1st reinforcer to the 10th reinforcer. Abscissa: Treatment conditions for the saline (n=8), ceftriaxone 100 mg/kg (n=9) and 200 mg/kg (n=12) groups. Paired student t-tests were used to compare Day 1 to Day 2 within each group. Vertical bars represent S.E.M.

Panel B. **In regards to motivated response rate, the mice in each group responded at the same rates to obtain the reinforcer suggesting that ceftriaxone treatment does not produce motor effects or alter motivation to obtain the reinforcer.** All groups of mice responded faster on Day 2 ($p < 0.05$) suggesting that consolidation and retention had occurred. Ceftriaxone treatment failed to alter the motivation or the speed to respond at either dose. Ordinate: Dipper response rate was calculated as the total number of center nose poke responses over session time. Vertical bars represent S.E.M. Other details as in Panel A.

Panel C. **By Day 2, all groups of mice learned to discriminate between the correct and incorrect nose-poke holes.** On Day 1, mice in all groups made incorrect responses in the inactive nose-poke holes. However, on Day 2, all groups of mice made significantly less incorrect responses ($p < 0.05$) indicating the mice could discriminate between the active and inactive responses. Ceftriaxone treatment failed to alter the discrimination measure at either dose relative to the saline control group. Ordinate: Mean activity rate was calculated as the total number of responses in both the left and right nose-poke holes divided by the total session time. Vertical bars represent S.E.M. Other details as in Panel A.

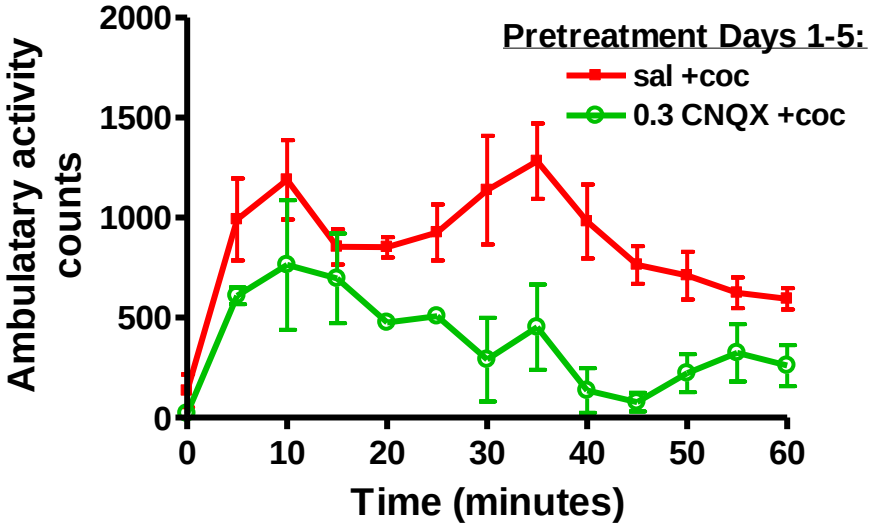

Fig. 6: Activity of rats given a challenge injection of cocaine on Day 12. Two groups of rats received microinjections of CNQX (0.3 ug/0.5 ul) or saline into the dorsolateral striatum 15 minutes prior to cocaine (20 mg/kg) once daily for 5 days (Days 1-5). After a 6-day drug-free period, all rats were challenged with cocaine (no intracranial injection) and ambulatory activity was measured for 60 minutes. Results demonstrate that CNQX reduced the development of behavioral sensitization to repeated cocaine administration. Mean ± SEM; N=4/group.

Research Project 8: Project Title and Purpose

Genetic Variations in Inflammation-Related Genes in Patients with Chronic Pelvic Pain Syndrome – The etiology and pathogenesis of Chronic Prostatitis/Chronic Pelvic Pain Syndrome (CP/CPPS) are unknown. The purpose of this study is to test the hypothesis that genetic polymorphisms of candidate genes *COMT, CGH1, IL10, TNF*, or *HMGB1* contribute to the development of CP/CPPS. We will also capture data on past medical history to assess whether specific medical conditions such as cardiovascular disease, hematologic disease and psychiatric conditions are associated with specific polymorphisms, and if these conditions define specific subgroups of patients with CP/CPPS. We will measure RNA and correlate with specific polymorphisms to confirm the mechanism of action.

Anticipated Duration of Project

12/1/2011 – 12/31/2012

Project Overview

The etiology and pathogenesis of Chronic Prostatitis/Chronic Pelvic Pain Syndrome (CP/CPPS) are unknown. Several candidate genes involved in chronic inflammation and/or chronic pain conditions (*COMT, CGH1, IL10, TNF*, and *HMGB1)* have been found to be genetically polymorphic. Our preliminary data indicates that the incidence of several of these polymorphisms are greater in patients with CP/CPPS than controls, either in the entire group of CP/CPPS patients, or correlating with specific aspects of past medical history. Therefore, in the current project, we plan to test the hypothesis that genetic polymorphisms of candidate genes *COMT, CGH1, IL10, TNF*, or *HMGB1* contribute to the development of CP/CPPS. We will also capture data on past medical history to assess whether specific medical conditions such as cardiovascular disease, hematologic disease and psychiatric conditions are associated with specific polymorphisms, and if these conditions define specific subgroups of patients with CP/CPPS.

Specific Aim 1: Test the hypothesis that genetic polymorphisms in candidate genes correlate with the incidence of CP/CPPS. This will be tested in a group of patients with CP/CPPS compared to a group of asymptomatic controls.
Specific Aim 2: Test the hypothesis that genetic polymorphisms in the promoter regions of candidate genes also modulate their expression, resulting in alterations in the level of level of mRNA.

Patients with CP/CPPS will be recruited from the PI's practice at Temple University. A group of age matched asymptomatic controls will also be recruited. Samples including saliva and blood will be drawn for obtaining DNA and RNA. Symptoms will be assessed using the NIH-Chronic Prostatitis Symptom index and a past medical history questionnaire developed for an NIH study of CP/CPPS. Inclusion, exclusion and deferral criteria will be the same as the NIH Prostatitis cohort study.

We plan to correlate the symptoms with the polymorphisms found, comparing patients with and

without CP/CPPS. Specific phenotypes of patients with CP/CPPS, i.e., those with specific items of past medical history, will be correlated with the frequency of polymorphisms. We will measure RNA and correlate with the polymorphism abnormalities to confirm that the polymorphisms are indeed causing alterations in RNA produced and to confirm the mechanism of action.

Principal Investigator

Michel A. Pontari, PhD
Professor of Urology
3401 North Broad Street
Suite 340, Zone C
Philadelphia, PA 19140

Other Participating Researchers

Evgeny Krynetskiy, PhD, John Gaughan, PhD – employed by Temple University

Expected Research Outcomes and Benefits

The relation of genotypes with corresponding phenotypes will help to prospectively define the functional significance of the SNPs and define the relationship between genetic polymorphisms and CP/CPPS. Findings include the possibility that some SNPs are different in all patients with CP/CPPS compared to controls, whereas others may only be found more frequently in CP/CPPS patients with certain medical problems, such as cardiovascular disease. To establish the mechanism, alterations in RNA need to be confirmed in patients who have the polymorphisms identified.

If proved true, these findings will help elucidate the molecular mechanisms leading to pelvic pain and define possible treatment strategies for this syndrome. CP/CPPS is a common condition, with very poor quality of life, and for which no standard therapy has been identified. The goal and significance of this project is to identify a mechanism of action that contributes to the symptoms of CP/CPPS and can be exploited in treatment. For example, if patients with CP/CPPS are found to be IL-10 deficient, then administering IL-10 becomes a potential therapy, as has been done in other inflammatory and pain syndromes. Differences in SNPs for the other genes are also potential therapeutic targets. It is possible that the identified SNPs could be used as markers. For example, if IL-10 correlates with both the presence of CP/CPPS and cardiovascular disease, then men with CP/CPPS who have IL-10 gene polymorphisms should also be screened for cardiovascular disease.

Summary of Research Completed

This project has been delayed. New start date of 12/01/2011.

Research Project 9: Project Title and Purpose

Characterization of the Effects of Hypertension on Adult Brain Neurogenesis – Our underlying hypothesis is that hypertension impairs neurogenesis by decreasing the number of neural stem cells (NCS) in the subventricular zone (SVZ) and the dentate gyrus leading to changes in intrinsic properties and functional characteristics. Changes in intrinsic properties that affect subsequent neural progeny turn-over and diminished growth factor support to the neuronal environment. No studies to date have directly evaluated the effect of hypertension on the neurogenic response. Besides the well known susceptibility of hypertensive individuals to stroke there is also strong correlation between hypertension and mild cognitive impairment. The NSC dysfunction in hypertension being studied here would shed light on explaining the occurrence of both mild cognitive dysfunction and poor stroke recovery when hypertension is present.

Anticipated Duration of Project

12/1/2010 – 6/30/2012

Project Overview

Aim 1: Evaluation of the direct effects of chronic hypertension on the neurogenic response in-vivo.

To understand how hypertension may induce changes to the NSC, we will first test whether administration of a slow pressor dose of Ang II for a given duration affects the number of proliferating NSC and viability. A comparative analysis of NSC proliferation and survival will be examined at the three most neurogenic areas (forebrain SVZ, hippocampal dentate gyrus and corpus callosum) to determine whether a particular brain region is more sensitive to the hypertensive condition. Since many NSC populations can be found in "stem cell niches" with proximity to the microvasculature, we will evaluate if a correlation can be established between NSC dysfunction and distance from the vasculature. The assessments in hypertensive animals will be compared to normotensive animals.

Aim 2: Effects of angiotensin II on BBB function and its impact on neural stem cell proliferation and multilineage differentiation in an in-vitro BBB model.

Our preliminary experiments have revealed that chronic hypertensive animals have disruptions to the blood-brain barrier (BBB), which exposes the neuronal environment to blood components. BBB permeability promotes deterioration of neuronal networks. It is therefore likely that BBB permeability could impact NSC viability and proliferation. To understand better the mechanism for which Ang II is affecting the BBB and the NSC, we have modeled this condition in-vitro. We will use primary mouse BMVEC, primary mouse astrocytes and primary mouse neural stem cells. We will perform co-culture experiments, using Boyden chambers, to place endothelial cells on a porous membranous surface (top chamber), astrocytes on the opposite side of the membrane and NSC on the lower chamber. We will then expose the endothelial cells to recombinant Ang II and evaluate the NSC for changes in viability and proliferation. Furthermore, we will evaluate how Ang II treated BMVEC alters NSC differentiation and determine the ratio and morphology of maturing astrocytes and neurons.

Principal Investigator

Tinatin Chabrashvili, MD, PhD
Assistant Professor; Department of Neurology
Temple University School of Medicine
3401 North Broad Street, C525
Philadelphia, PA, 19140

Other Participating Researchers

Servio Heybert Ramirez, PhD, Jan-Michelle Malette BS, Ming Zhang MD, PhD – employed by Temple University

Expected Research Outcomes and Benefits

The findings of our project will shed light on how vascular and neural stem cells communicate in health and in disease, specifically in the context of hypertension. The results of this project will determine whether chronic hypertension affects the neural stem cell survival, differentiation, intrinsic properties and function in the adult brain. Targeting these negative regulators will help us to design new therapeutic measures to prevent morbidity and mortality provoked by the detrimental effects of hypertension, especially stroke and dementia. In particular, it will help us to design the therapeutic tools to promote repair and neural plasticity to improve stroke outcome and memory. It will also help us to determine the way to protect the neural stem cells through improving neurovascular coupling and BBB integrity at the neurovascular niche.

Summary of Research Completed

At this phase of the research, we have further developed the animal model, which is used by us to study the impact of high blood pressure on adult brain neurogenesis, including in the context of ischemic stroke. This is especially important since hypertension is a major risk factor for stroke and cognitive impairment. There is recent experimental evidence that stroke induces neurogenesis, which affects the final outcome and recovery from stroke.

As our ischemic stroke model, we mastered the middle cerebral artery permanent occlusion model (MCA) with modification. Briefly, the mouse is anesthetized with 1:1 ketamine/xylazine and the right side of the head is shaved. The animal is place on its left side. A 5 cm vertical skin incision is made posterior to the orbit and the skin is reflected posteriorly. A horizontal incision is made along the linea temporalis, where the temporalis muscle attaches to the skull. The temporalis is gently dissected away from the skull. While pulling inferiorly on the temporalis muscle, an 18.5 gauge needle is used to manually make 4 holes around the skull over the middle cerebral artery. The MCA should be visible through the translucent skull. Fine forceps are used to ronguer away the bone between the four drilled holes and the piece of skull overlying the MCA is removed. Gently, a thermal cauterize is used to coagulate the MCA. Once the MCA appears black, it is fully transected using surgical scissors. The temporalis muscle and skin are returned to their original locations and staples are used to close the skin wound. Using this model we are achieving stroke volume approximately 18.99 mm^3 (Fig. 1), which is significant by size

and anatomical distribution to evaluate the stroke induced neurogenesis in hypertensive mice and to compare it with normotensive mice neurogenesis.

We completed the studies characterizing the role of high blood pressure on the cerebral microvasculature, blood-brain barrier (BBB), and role of oxidative stress on the function of blood-brain barrier permeability, which we published in *"Neuroscience" (*Zhang M, et al.: Neuroscience: 2010, 171(3):852-8). The functional status of cerebral microvessels and integrity of BBB could be essential, since the adult neural stem cells reside in neurovascular niche.

In this part of the study we found the key mechanisms by which Angiotensin II (AngII) mediates cerebral microvascular inflammation. C57BL/6 male mice were subjected to slow-pressor dose of AngII infusion using osmotic mini-pumps at a rate of 400ng/kg/min for 14 days. Vascular inflammation in the brain was evaluated by analysis of leukocyte-endothelial interaction and BBB permeability. Results from intravital microscopy of pial vessels in-vivo, revealed a 4.2 fold ($p<0.05$, compared to vehicle) increase in leukocyte adhesion on day 4 of AngII infusion. This effect persisted through day 14 of AngII infusion, which resulted in a 2.6 fold ($p<0.01$, compared to vehicle) increase in leukocyte adhesion. Furthermore, evaluation of BBB permeability by Evans blue extravasation showed that Ang II significantly affected the BBB, inducing 3.8 times ($p<0.05$, compared to vehicle) higher permeability. Previously we reported that AngII mediated hypertension promotes oxidative stress in the vasculature. Thus, we used the superoxide scavenger; 4-hydroxy-TEMPO (Tempol) to determine whether AngII via oxidative stress could contribute to higher leukocyte adhesion and increased BBB permeability. Tempol was given via drinking water (2mmol) on day 4 following Ang II infusion, since oxidative stress increases in this model on day 4. Treatment with Tempol significantly attenuated the increased leukocyte/endothelial interactions and protected the BBB integrity on day 14 of AngII infusion. In conclusion, AngII via oxidative stress increases cerebral microvasculature inflammation and leads to greater immune-endothelial interaction and higher BBB permeability.

Currently, we are undertaking the experiments to complete the assessment of neurogenesis in the context of hypertension at baseline and during the additional pathological challenge - Ischemic Stroke.

Part of the experiments under Aim 2 relates to the study of how the BBB changes while under the insult of Angiotensin II. Since these characterizations have been recently published by us (Zhang M. *et. al.*), we are now expanding our studies to include other possible pharmacological interventions that can be used to provide protection to the BBB.

In the next phase of the study we will evaluate how barrier protective agents such as antioxidants or pharmacological ligands of the cannabinoid receptors provide protection of stem cell niches by restoration of BBB function in hypertension.

To this end, we have completed a study (currently under review in the *Journal of Neuroscience*) that provides compelling evidence that activation of the endogenous cannabinoid system by pharmacological activation of the cannabinoid 2 receptor (CB2R) renders BBB protection. Figure 1 shows the assessment of BBB leakiness and integrity as measured by trans-endothelial electrical resistance (TEER). Primary human brain microvascular endothelial cells (BMVEC)

were grown on ECIS array electrodes and TEER was monitored continuously over the course of 24 and 36 hrs (Figure 2A, B and C). Treatment of BMVEC monolayers with *E.coli* LPS (50 ng/ml) induced a rapid drop in resistance (80% of control) over time, which was significantly attenuated by a novel synthetic CB2R agonist, O-1966 (Figure 1A, $P<0.05$). These data indicate that CB2R stimulation can provide BBB protection under inflammatory insult (LPS). The next set of experiments were designed to understand whether CB2R activation could increase barrier structural integrity under physiologic conditions. Indeed, application of the highly selective CB2R agonists (O-1966 or JWH-133) resulted in dose- and time-dependent augmentation of tightness of BMVEC monolayers (11-15%, $P<0.05$, Figure 2B,C). Although various signaling mechanisms can influence BBB tightness, the culminating effect is on the tight junctions (TJ) located between brain endothelial which form the BBB. Therefore, TJ protein expression in BMVEC was evaluated after treatment with CB2R agonists. Four-hour stimulation of CB2R with O-1966 or JWH133 caused a 2.2-2.7 fold increase in the amount of the TJ proteins occludin and claudin-5 (Fig. 3A,B) present in the membranous fraction of BMVEC lysates. Longer exposure to JWH133 resulted in further increases in occludin (3.8 fold) and claudin-5 (2.8 fold), while O-1966 increased only by 50% and claudin-5 by 20% when compared to untreated controls. In summary, these results suggest that the CB2R protective effects on BBB function are mediated in part by increased expression of TJ proteins in brain endothelium.

Our future plans include the examination of the CB2R agonists in hypertensive animals and its effects on BBB permeability and on the NSC niches.

Publication Related To The Grant

1- Zhang M, Mao M, Ramirez SH, Tuma R, Chabrashvili T. Angiotensin II Induced Cerebral Microvascular Inflammation and Increased Blood-Brain Barrier Permeability via oxidative stress: Neuroscience: 2010, 171(3):852-8

2- Barry J, Patel M, Faro F, Mohamed F, Sawaya BE, Chabrashvili T: Implications Of Vascular Burden In Dementia: Does It Come Down To The White Matter? International Stroke Conference 2012: Abstract 12-ISC-A-2551-AHA

Fig. 1

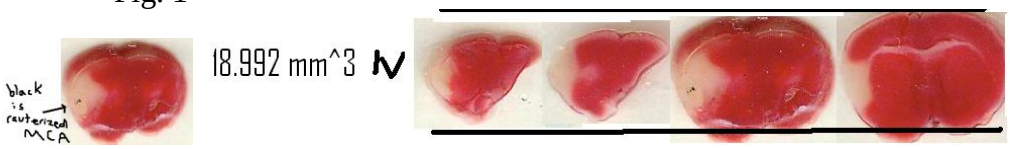

Fig. 2

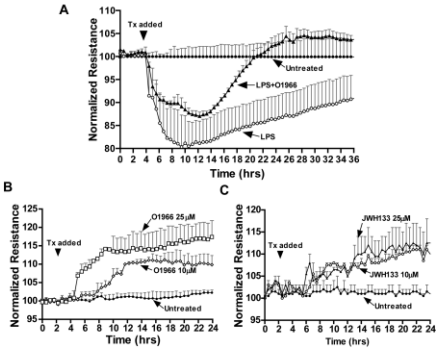

Fig. 3

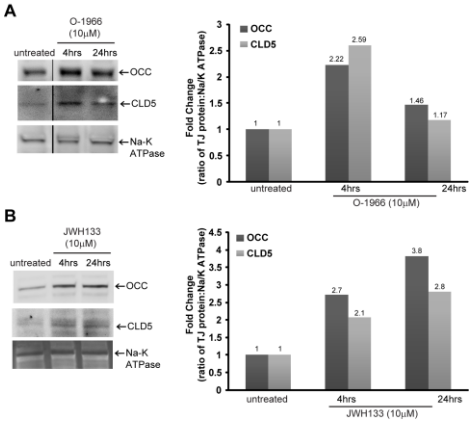

Research Project 10: Project Title and Purpose

PDMD: A Complex II-Regulated Form of Mitochondrial Dysfunction in Exhausted Cells – Functional impairment of mitochondria contributes to many human diseases including myocardial infarction, stroke, cancer and aging. However, the underlying mechanisms of mitochondrial dysfunction are not well understood. Our preliminary studies elucidate a mode of mitochondrial depolarization that is independent of cyclophilin D, Bcl-2 family proteins, extra mitochondrial energy, or high amplitude swelling. We termed this mode of mitochondrial dysfunction proton-dependent mitochondrial depolarization (PDMD), which prominently manifests in ischemic cells. The evolutionarily conserved PDMD is dependent on dissipation of the mitochondrial potential and can be reversed by the mitochondrial substrate. This route of reversible mitochondrial impairment provides a potential target for rejuvenation of exhausted cells in acute injury.

Anticipated Duration of Project

12/1/2010 – 12/31/2011

Project Overview

The primary function of mitochondria is the production of ATP, for which the main driving force of synthesis depends on the intermembrane space electrochemical proton gradient that is maintained by the highly selective mitochondrial inner membrane. Consequently, dissipation of this proton gradient causes mitochondrial depolarization. This depolarization occurs following Ca^{2+} overload, ROS overproduction, cyclophilin D-dependent permeability transition pore (PTP) opening, pro-apoptotic Bcl-2 family protein outer membrane permeabilization, and dissipation of

the proton gradient by uncouplers. Owing to their importance in mitochondrial physiology, the mechanisms of PTP, Bcl-2, and microbial toxin(s)-dependent depolarization have been extensively studied. However, despite this intense research focus, regulation and manipulation of these mechanisms have not afforded reliable clinical successes for human diseases including myocardial infarction, stroke, cancer, aging and neurodegeneration, all of which have been linked with mitochondrial dysfunction. In an attempt to better understand mitochondrial physiology, we simplified our research question to focus on the basic mechanism of how the mitochondrial proton gradient is maintained, how it can be dissipated, and ultimately, how it can be re-established. *For the first time, our studies elucidate a mode of mitochondrial depolarization that is independent of cyclophilin D, Bcl-2 family proteins, extra mitochondrial energy, and high amplitude swelling. We termed this mode of mitochondrial dysfunction proton-dependent mitochondrial depolarization (PDMD).* Our novel observation led us to generate three fundamental questions regarding PDMD. *First*, what is the role of PDMD in mitochondrial physiology? *Second*, does the re-establishment of the proton electrochemical gradient restore mitochondrial function? And *third*, is PDMD a primary mechanism of cell injury? To answer these questions, we propose to employ classical biochemical and cell biological approaches. Further, our innovative research design will address whether PDMD represents a point of irreversibility in mitochondrial physiology, or instead can be reversed under certain conditions by supplementation of the complex II substrate succinate.

Principal Investigator

Madesh Muniswamy, PhD
Assistant Professor
Temple University School of Medicine
627 Kresge Building
3440 N. Broad Street
Philadelphia, PA 19140

Other Participating Researchers

Varsha Daswani – employed by Temple University

Expected Research Outcomes and Benefits

We believe that coupling the re-examination of previous controversial findings using modern techniques will significantly reduce the chance for erroneous results. We expect that our findings will offer evidence on three important points: first, that evolutionarily conserved PDMD is reversible and solely dependent upon mitochondrial complex II; second, that PDMD is neither an apoptotic nor necrotic phenomena but, rather, is a form of mitochondrial exhaustion; and third, that Succinate-mediated restoration of mitochondrial function can reduce the damage associated with myocardial infarction. This final point is important in that it sets the stage for future studies aimed at the acute delivery of Succinate for the reversal of mitochondrial exhaustion and restoration of cell function during acute myocardial infarction. By maintaining cardiac function during ischemia, Succinate may prove an ideal therapy to preserve myocardium until revascularization by Percutaneous Coronary Intervention (PCI) or fibrinolytics is initiated.

Summary of Research Completed

Specific Aim 1: Characterize the role of PDMD in mitochondrial physiology

A). *Role of individual ETC complexes in $\Delta\Psi_m$ maintenance and activation of PDMD.*
The complex II pathway preserves the membrane potential in the absence of complex I activity. As Succinate afforded protection from $\Delta\Psi_m$ loss during pseudo-hypoxia, we next chose to investigate the discrete role of complex II in $\Delta\Psi_m$ maintenance. To assess the contribution of individual mitochondrial complexes to the $\Delta\Psi_m$, permeabilized rat pulmonary microvascular endothelial cells (RPMVECs) were supplemented with complex-specific mitochondrial substrates either alone or in combination with mitochondrial complex and F_0F_1-ATPase inhibitors. Following permeabilization, cells exhibit $\Delta\Psi_m$ loss due to lack of available substrates as the cytoplasmic contents diffuse and dilute into the experimental buffer (data not shown). Surprisingly, the complex II substrate succinate (Succ), but not the complex I substrates malate and glutamate (Mal/Glut), effectively maintained $\Delta\Psi_m$ in response to permeabilization (Fig. 1A). Succ also prevented $\Delta\Psi_m$ loss even in the presence of the F_0F_1-ATPase inhibitor Oligomycin, which expectedly blocked the protective effect of ATP on $\Delta\Psi_m$ maintenance (Fig. 1B). Further, the effect of Succ on $\Delta\Psi_m$ maintenance was not affected by the complex I inhibitor Rot (Fig. 1C), excluding the possibility that Succ initiates proton pumping via the reverse flow of electrons through complex I, and was completely abolished by the non-metabolizable complex II competitive inhibitor malonate (Mao) (Fig. 1D). However, Succ did not offer protection from complex III-mediated $\Delta\Psi_m$ loss in the presence of the inhibitors myxothiazol and antimycin A (Fig. 1E and F). In particular, antimycin A induced immediate $\Delta\Psi_m$ loss even in the combined presence of Succinate and ATP, which hyperpolarizes the membrane, suggesting that complex II requires the proton pumping capability of mitochondrial complex III in order to establish $\Delta\Psi_m$. This initial observation raises the possibility that complex II pathway may be sufficient to establish $\Delta\Psi_m$ in the absence of complex I.

B). *Role of PDMD in hypoxic condition:* To assess establishment of $\Delta\Psi_m$ during hypoxic conditions, we chose to utilize freshly isolated murine cardiomyocytes as these cells are a primary target of hypoxic damage in humans during myocardial infarction. Chemical inhibition of complexes I and IV (Rot/Oligo) induced rapid $\Delta\Psi_m$ loss in cardiomyocytes that was similar to other cell types that could be reversed by Succ supplementation (Fig. 2A). To directly assess the relationship between $\Delta\Psi_m$ loss and hypoxia, $\Delta\Psi_m$ was assessed following cell permeabilization in hypoxic experimental buffer. Marked $\Delta\Psi_m$ loss was observed when cells were permeabilized in this buffer (Fig. 2B), the hypoxic status of which was verified by probing for HIF-1α stabilization after 5 hr (Fig. 2C).

C). *Is PDMD evolutionarily conserved throughout the eukaryotic system?* To further characterize the role of complex II in the $\Delta\Psi_m$, we next assessed whether reintroduction of the complex II substrate Succ could restore $\Delta\Psi_m$ after complete dissipation of the proton gradient ($\Delta\Psi_m$ loss). Following permeabilization-induced $\Delta\Psi_m$ loss, cells were supplemented with either a combination of complex I substrates (Mal/Glut or Mal/Pyr) or Succ. In contrast to Mal/Glut or Mal/Pyr, addition of Succ resulted in dramatic $\Delta\Psi_m$ restoration (Fig. 3A). Because complex I

substrates were ineffectual at maintaining $\Delta\Psi_m$, we developed a rapid chemical means to further test the efficacy of complex II in mitochondrial function and mimic hypoxia in normoxic cells. Cells were supplemented with Mal/Glut and then $\Delta\Psi_m$ loss was induced by a combination of Rot/Oligo, completely eliminating the contribution of complex I (via secondary ATP production) as well as intermembrane space proton loss through F_0F_1-ATPase. Cells were then treated with the complex II substrate Succ and extramitochondrial ATP alone or in combination. This approach (Succ versus ATP) allowed us to distinguish between proton gradient maintenance by Succ or glycolytic ATP, and to directly monitor $\Delta\Psi_m$ recovery. The chemical combination of Rot/Oligo triggered rapid $\Delta\Psi_m$ loss, which could be reversed by supplementation with Succ in several cell types that we have examined (mouse, rat, and human pulmonary microvascular endothelial cells (MPMVEC, RPMVEC, and HPMVEC, respectively), C2C12 myoblast, and S2 drosophila cells) (Fig. 3B, C, F). Complex III inhibition resulted in $\Delta\Psi_m$ loss that could not be rescued by the proton-pumping capabilities of complex I alone. While ATP in combination with Succ produced an additive effect on $\Delta\Psi_m$, ATP alone did not reverse $\Delta\Psi_m$ loss (Fig. 3B). The fatty acid β-oxidation end-product acetyl CoA is a major fuel in some tissues, and ultimately enters the citric acid cycle where it will increase all TCA cycle metabolites, including Succ and Mal. However, Rot/Oligo-induced $\Delta\Psi_m$ loss was not affected by acetyl CoA supplementation (Fig. 3C). Addition of the citric acid cycle metabolite α-ketoglutarate also did not restore $\Delta\Psi_m$, despite being a precursor of Succ in the TCA cycle (Fig. 3C). In addition to Rot/Oligo, $\Delta\Psi_m$ loss also occurred following addition of the complex II competitive inhibitor Malonate (Mao). Subsequent addition of the complex I substrates Mal/Pyr and their essential cofactor NAD+ did not restore $\Delta\Psi_m$ (Fig. 3D), indicating a rapid effect of Succ in the establishment of the $\Delta\Psi_m$. Although our data demonstrate the restoration of $\Delta\Psi_m$ by Succ following $\Delta\Psi_m$ loss, there is a possibility that restoration of $\Delta\Psi_m$ by Succ is actually due to the secondary generation of NADH from mitochondria. To address this issue, we simultaneously measured both $\Delta\Psi_m$ and NADH generation in permeabilized cells. Inhibition of complex I by Rot rapidly increased cellular NADH levels but did not affect $\Delta\Psi_m$ as detected by TMRE fluorescence. However, subsequent addition of Succ rapidly increased $\Delta\Psi_m$ (as indicated by a decrease in TMRE as more dye sequesters into the mitochondria) without an appreciable effect on NADH generation (Fig. 3E). Conversely, Mal/Glut did not increase $\Delta\Psi_m$ when complex II was inhibited by Mao despite a robust increase in cellular NADH levels. Because Succ-mediated electron transfer relies on complex III (Fig. 2E and F), we next assessed whether bypass of complex II/III by delivery of the complex IV substrates tetramethyl-*p*-phenylenediamine (TMPD) and ascorbate (Asc) could preserve $\Delta\Psi_m$ in response to a combined complex I/F_0F_1-ATPase inhibition (Rot/Oligo). TMPD/Asc supplementation only partially restored $\Delta\Psi_m$ (Fig. 3F). However, unlike the dose-dependent response seen with Succ, addition of a higher concentration of TMPD/Asc was toxic to mitochondria and $\Delta\Psi_m$ maintenance.

<u>Specific Aim 2: Does the re-establishment of the proton electrochemical gradient restore mitochondrial function?</u>

A). *<u>Does cyclophilin D inhibition re-establish the $\Delta\Psi_m$ following PDMD?</u>*
Rot/Oligo-induced mitochondrial depolarization was not prevented by the PTP blocker cyclosporine A (CsA), but subsequent addition of the complex II substrate succinate (Succ) substantially restored $\Delta\Psi_m$. Pretreatment with CsA also did not prevent Rot/Oligo-induced $\Delta\Psi_m$

loss, although it significantly blunted Ca^{2+}-dependent mitochondrial depolarization via the PTP open even in the presence of Succ, indicating that Succ cannot prevent opening of the PTP. In parallel, Succ supplementation did not prevent $\Delta\Psi_m$ loss triggered by the mitochondrial swelling-inducing agent alamethicin.

B). *Is PDMD a Bcl-2 family protein-associated mechanism?*

Next, it was of interest to determine whether Rot/Oligo-induced $\Delta\Psi_m$ loss is similar to mitochondrial depolarization caused by pro-apoptotic Bcl-2 family proteins. A logical assumption would be that the mitochondrial proton gradient can be maintained if complex III and complex IV are intact and cytochrome c is present to enable electron transfer from complex III to IV. During apoptosis, cytochrome c is released from the intermembrane space via a Bax/Bak-dependent mechanism that precedes $\Delta\Psi_m$ loss. Rot/Oligo-induced $\Delta\Psi_m$ loss is a Bcl-2 independent phenomenon. $\Delta\Psi_m$ loss by the pro-apoptotic protein tBid (caspase-8-cleaved), an activator of Bax and Bak, is not rescued by Succ. This observation suggests that cytochrome c is essential for normal $\Delta\Psi_m$ maintenance initiated by complex II. Similar to other cell types, WT and *bax*$^{-/-}$*bak*$^{-/-}$ double KO fibroblasts underwent Succ-reversible $\Delta\Psi_m$ loss even in the presence of CsA. Our data suggests that Rot/Oligo-induced mitochondrial depolarization is neither an apoptotic (Bcl-2-mediated) nor a necrotic (PTP opening) phenomenon, and thus should not exhibit mitochondrial cytochrome c release. Unlike tBid (100 nM), Rot/Oligo-induced depolarization did not trigger cytochrome c release after 20 min exposure. These results demonstrate that Rot/Oligo induces $\Delta\Psi_m$ loss by mechanisms not directly dependent upon Bcl-2 or PTP opening and suggests that mitochondrial membrane potential may be manipulated during hypoxia via the availability of specific metabolic substrates. Currently, the proposed aims are under progress.

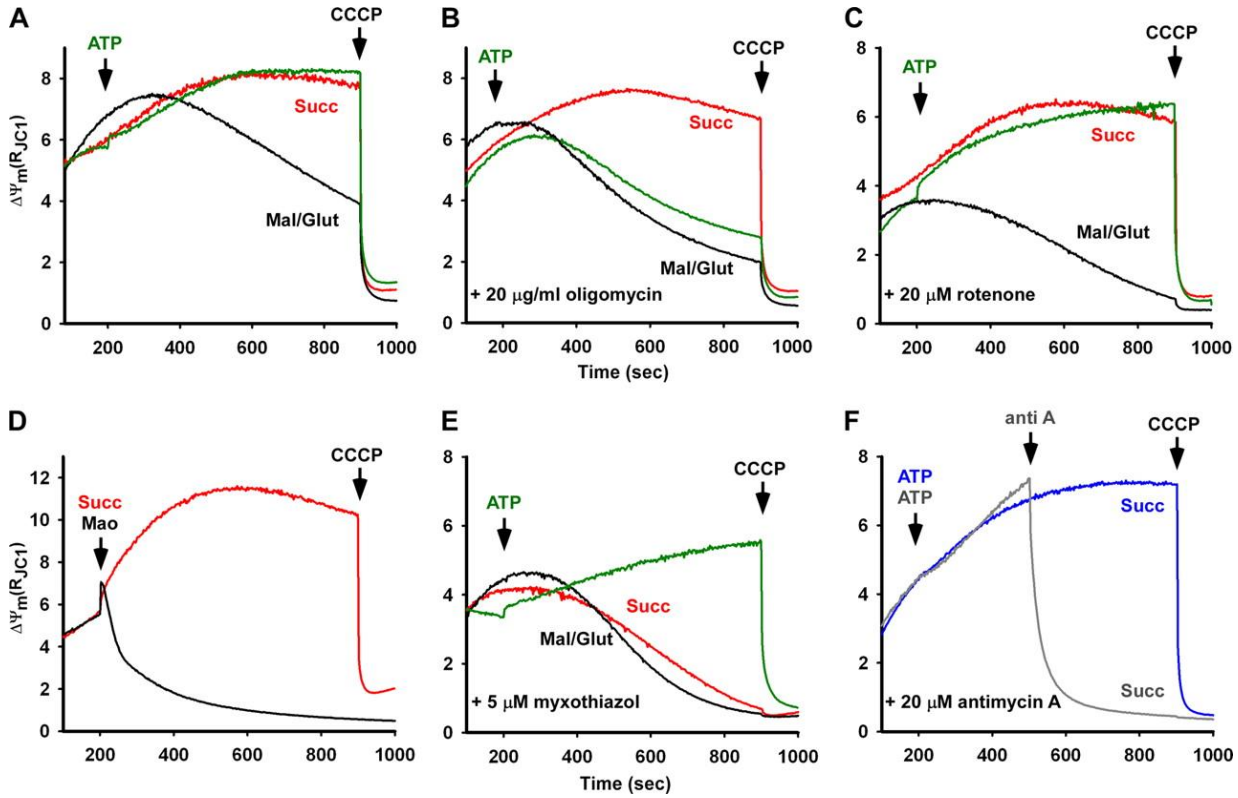

Fig. 1. Mitochondrial complex II establishes the membrane potential in permeabilized cells. Succinate (Succ; 2 mM) but not malate/glutamate (Mal/Glut; 1 mM/1 mM) maintained $\Delta\Psi_m$ in digitonin-permeabilized RPMVECs under (A) control cells and (B) in the presence of the F_0F_1-ATPase inhibitor oligomycin (Oligo; 20 μg/ml). ATP (100 μM) was effective only in the absence of oligomycin. (C) Complex I inhibition by rotenone (Rot; 20 μM) does not affect Succ-mediated $\Delta\Psi_m$ maintenance but (D) the complex II inhibitor malonate (Mao; 2 μM) abolished Succ-dependent $\Delta\Psi_m$. Succ afforded no protection from complex III inhibition by (E) myxothiazol (5 μM) or (F) antimycin A (20 μM). Arrows indicate the addition of different molecules at various intervals. The mitochondrial uncoupler CCCP was added at the indicated time to dissipate the membrane potential.

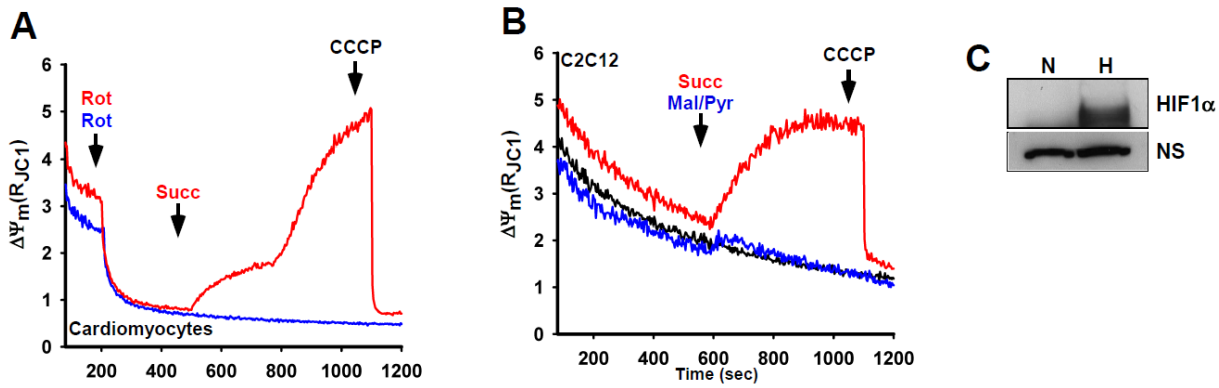

Fig. 2. Preservation of mitochondrial membrane potential by Succ-mediated metabolism during hypoxia. Both (A) chemical- and (B) hypoxic-induced $\Delta\Psi_m$ loss is reversed by Succ but not Mal/Pyr in freshly isolated permeabilized, mature murine cardiomyocytes and C2C12 cells, respectively. (C) Hypoxic status was confirmed by HIF-1α stabilization in C2C12 cells following 5 hr of hypoxia (NS; non specific).

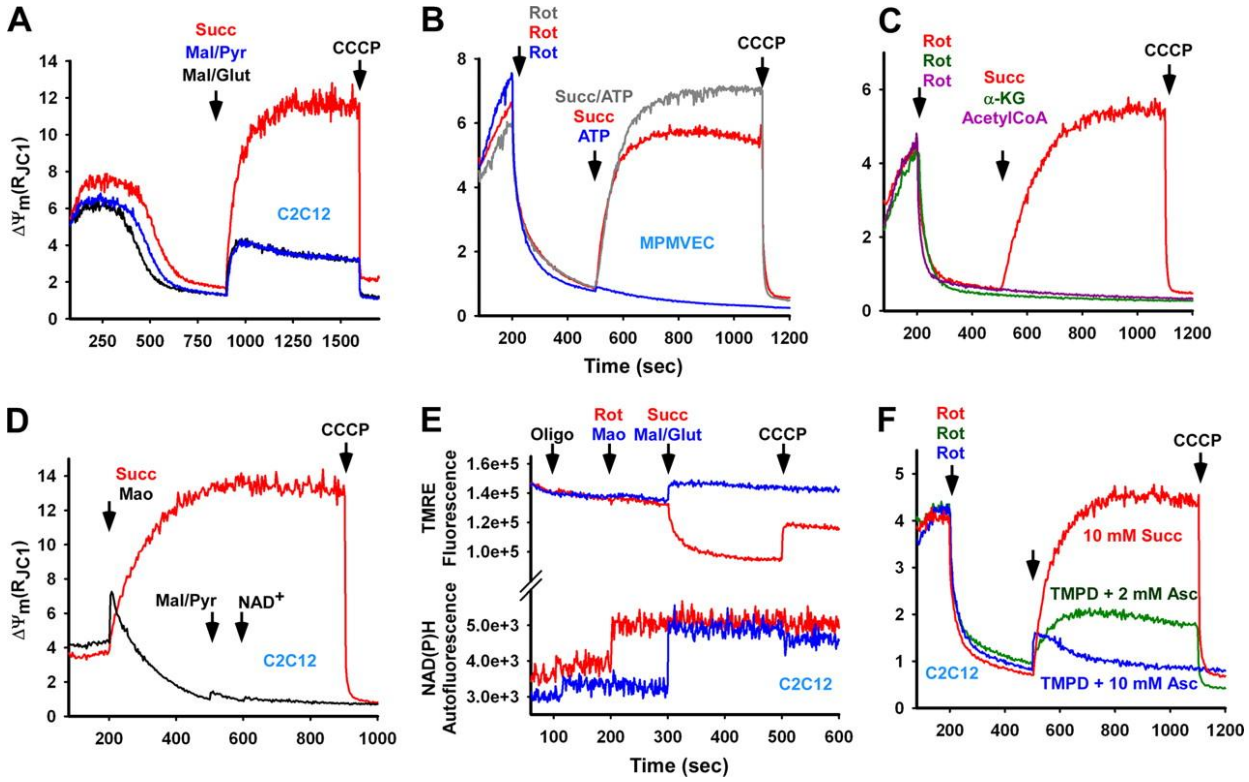

Fig. 3. Complex II substrate restores $\Delta\Psi_m$ during complex I and F_0F_1-ATPase inhibition. (A) Differential effects of Complex II (Succ; 10 mM) and Complex I (Mal/Glut; 5 mM/5 mM, Mal/Pyr; 5 mM/5 mM) substrates on reestablishment of $\Delta\Psi_m$ in murine myoblast (C2C12) cell line. (B) $\Delta\Psi_m$ depolarization caused by complex I and F_0F_1-ATPase inhibition (Rot/Oligo; 20 μM/ 20 μg/ml) could be reversed by Succ (10 mM) in MPMVECs. (C) The citric acid entry

substrate Acetyl CoA (AcetylCoA; 5 mM), and the Succ precursor α-ketoglutarate did not restore $\Delta\Psi_m$ in HPMVECs. (D) Mao-induced $\Delta\Psi_m$ depolarization was not reversed by combination of the complex I substrates Mal/Pyr (5 mM/5 mM) and the cofactor NAD^+ (100 μM). (E) An increase in NADH production in response to Mal/Glut (5 mM/5 mM) did not restore $\Delta\Psi_m$ in response to complex II inhibition by Mao (2 mM). (F) The complex IV substrates TMPD/Asc do not effectively reestablish $\Delta\Psi_m$ following Ros/Oligo-induced $\Delta\Psi_m$ loss. Oligo was added at 80 sec in B, C, D, and F. Arrows indicate the addition of different molecules at various intervals.

Research Project 11: Project Title and Purpose

Role of the B55α Protein Phosphatase 2A Holoenzyme in Modulating the Phosphorylation of p107 and Related Proteins – Members of the retinoblastoma family of growth suppressor proteins are inactivated via phosphorylation by cyclin dependent kinases (CDKs) in mid-G1 through mitosis. Hyperphosphorylation of these proteins inactivates them as repressors of E2F-dependent transcription and prevents interaction with other proteins. Pocket protein phosphorylation is challenged through the cell cycle by protein phosphatase 2A (PP2A), and we have recently identified a trimeric PP2A holoenzyme containing the regulatory B55α subunit that dephosphorylates p107 and p130. The purpose of this work is to characterize this complex in reactivation of pocket proteins in response to anti-mitogenic signals, as tumor cells are often refractory to anti-mitogenic signaling.

Anticipated Duration of Project

12/1/2010 – 8/31/2011

Project Overview

The retinoblastoma family of growth suppressor proteins consists of the tumor suppressor pRB and the functionally and structurally related proteins p107 and p130. p107 and p130 have been implicated in tumorigenesis in mouse knockout models where either p107 or p130 are simultaneously knocked out together with ablation of a pRB allele. These compound mice exhibit tumor patterns that are distinct from those seen in pRB heterozygous mice. Also, simultaneous inactivation of p107/p130 has shown that these proteins are critical for cell cycle exit in chondrocytes during development and for endochondral bone formation. When hypophosphorylated, pocket proteins bind and inactivate the E2F family of transcription factors, which are required for cell cycle regulated gene expression. Hypophosphorylated p107 has also been implicated in regulating TGF-β signaling, as p107 complexes with SMADS and translocates to the nucleus to modulate gene expression. These functions of pocket proteins are inactivated via phosphorylation by CDKs. CDKs are activated in mid to late G1 upon mitogenic stimulation of hyperphosphorylating pocket proteins. This results in disruption of their association with E2F transcription factors and other proteins. Pocket proteins remain hyperphosphorylated during the cell cycle and are abruptly dephosphorylated in mitosis and early G1 by PP1, coinciding with inactivation of CDKs. We have previously shown that PP2A plays a role in restricting the phosphorylation of pocket proteins through the cell cycle, which results in their rapid dephosphorylation when the activity of CDKs is compromised. PP2A

enzymes are Ser/Thr protein phosphatases that consist of a catalytic and a scaffold subunit that complex to a regulatory B subunit, which is responsible for substrate specificity and subcellular localization. There are four different families of B subunits, each with multiple members. We have recently identified a trimeric holoenzyme that dephosphorylates p107 and p130. B55α is the regulatory subunit of this trimeric holoenzyme. We have shown direct association of B55α with p107, and dephosphorylation of p107 by the trimeric holoenzyme *in vitro*. We have found that overexpression of B55α induces p107 dephosphorylation while its knockdown induces hyperphosphorylation. The aims of this study are: (1) To determine if endogenous p107 interacts with endogenous B55α in a variety of cells and/or upon certain stimuli. (2) To identify domains in B55α critical for binding to p107. (3) To determine if B55α is required for FGFα-induced dephosphorylation of p107 in chondrocytes.

Principal Investigator

Xavier Graña, PhD
Associate Professor of the Fels Institute and the Dept. of Biochemistry
Rm 308, AHP Bldg.
3307 N. Broad Street
Philadelphia, PA 19140

Other Participating Researchers

Alison Kurimchak – employed by Temple University

Expected Research Outcomes and Benefits

Pocket proteins are growth suppressor proteins that operate in a pathway that is almost invariably disrupted in human cancer. Often transforming alterations of this pathway are associated with hyperactivation of CDKs resulting from amplification of cyclin genes or CDKs, mutations on CDKs rendering them resistant to the action of CDK inhibitors, or inactivation of various members of either family of CKIs (CDK inhibitors). While PP2A has now been recognized as a tumor suppressor, its inactivation during cellular transformation has not been linked to alterations in the phosphorylation status of pocket proteins. However, our preliminary data show that an oncogene required for transformation of human cells, SV40 small t antigen, alters the phosphorylation of pocket proteins via inhibition of PP2A. Gaining insight on the particular PP2A complexes that modulate pocket proteins would permit future inquires on the involvement of deregulation of these complexes in mediating the alterations on pocket protein phosphorylation seen in certain tumor cells.

On the other hand, a PP2A holoenzyme sensitive to a simian virus 40 st and adenovirus E4ORF4 has been implicated in triggering p107 dephosphorylation upon stimulation of chondrosarcoma rat cells with FGFα. This dephosphorylation appears to be required for cell cycle exit in chondrocytes. Given that p130 and p107 are required for endochondral bone formation and chondrocyte cell cycle exit during development, our studies may implicate B55α in endochondral bone formation, a process that when defective leads to bone abnormalities in humans, thus, providing insight in a process that is not well understood.

Summary of Research Completed

We have already accomplished aims 1 and 2 and are currently attempting to complete aim 3. The aims of this study as originally planned were:

(1) To determine if endogenous p107 interacts with endogenous B55α in a variety of cells and/or upon certain stimuli.

We have completed this aim by demonstrating the endogenous interaction of the B55α PP2A holoenzyme and p107 in untreated human U-2 OS cells (Fig. 1) and reported these findings in Jayadeva et al. (2010). Anti-p107 antibodies efficiently co-immunoprecipitated PP2A/A and PP2A/C, whereas B55α was co-precipitated to a lower extent. B55α antibodies, which could not preclear B55α from the lysates, immunoprecipitated low levels of p107 that were above background detection (Fig. 1). These data indicate low abundance of endogenous complexes, Which may be due to the instability of the enzyme-substrate interaction. In addition, we have also followed up this observation and demonstrated the endogenous interaction of the B55α PP2A holoenzyme and p107 in exponentially growing rat RCS chondrosarcoma cells (data not shown). Importantly, stimulation of these cells with FGF1 induces formation of this complex coinciding with p107 dephosphorylation (data not shown). These unpublished data will be shown in our final report.

(2) To identify domains in B55α critical for binding to p107.

We have identified a residue in B55α, D197, which is essential for binding to p107 (Fig. 2). We have also found that p107 makes contact with B55α through at least two separate domains (data not shown). These data have been reported in Jayadeva et al. (2010). B55α consists of seven WD40 domains that form the blades of a β-propeller and a β-hairpin arm (Fig. 2A). p107 interacted both with the amino-terminal 1–216-amino acid fragment that contains the first three WD40 domains and the 217–447-amino acid C terminus fragment that contains the last four WD40 domains in cotransfection assays in U-2 OS cells (supplemental Fig. 2). However, these deletion forms of B55α poorly interacted with PP2A/C (Fig. 2A) and PP2A/A (not shown). It has been recently reported that β-catenin, a substrate of B55α, also interacts with both domains (Zhang et al., 2009). These results suggest that B55α substrates may make multiple contacts with the β-propeller structure. We also generated a series of point mutants targeting amino acids in the acidic top face of the β-propeller that have been previously found to be important for dephosphorylation of Tau by B55α (Xu et al., 2008). Fig. 2B shows that only residue Asp-197 was essential for binding to p107 in reciprocal immunoprecipitation assays from lysates of transfected cells with the indicated constructs. This residue was also clearly key for binding of B55α to PP2A/A and PP2A/C. Therefore, Asp-197 is critical for both formation of an holoenzyme and p107 recruitment. It also appeared that substitution of residue Lys-48 reduced binding to p107 despite efficient binding to PP2A/A and PP2A/C (Fig. 2B). It is important to note that this B55α point mutant is an excellent tool for further functional studies.

(3) To determine if B55α is required for FGFα-induced dephosphorylation of p107 in chondrocytes.

We have designed various siRNAs targeting rat B55α and are currently determining whether B55α knockdown prevents FGF1-induction of p107 dephosphorylation.

Publications

Jayadeva, G., Kurimchak, A., Garriga, J., Sotillo, E., Davis, A. J., Haines, D. S., Mumby, M., and Graña, X. (2010). B55alpha PP2A holoenzymes modulate the phosphorylation status of the retinoblastoma-related protein p107 and its activation. J Biol Chem 285, 29863-29873.

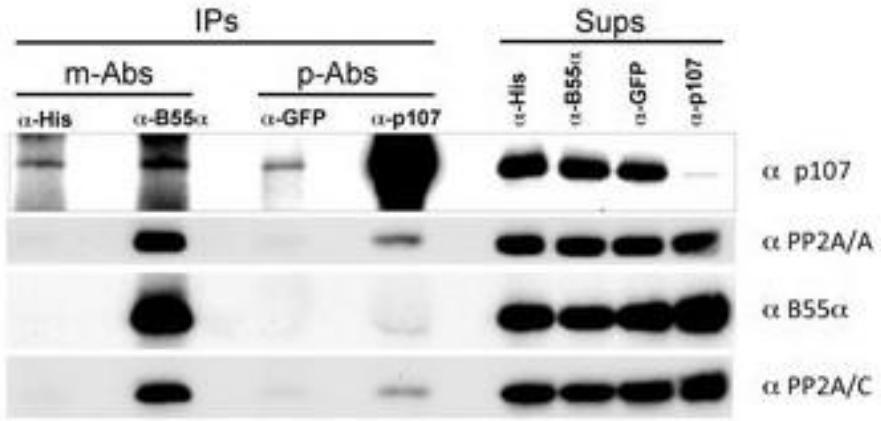

Fig 1. p107 interacts with trimeric B55α PP2A complexes in human U-2 OS cells.
Low levels of endogenous B55α and p107 are detected in U-2 OS cells. Complexes were immunoprecipitated with α-p107, α-B55α or control antibodies after overnight pre-clearing of cell lysates (1 mg) with control antibodies. Complexes were resolved via SDS-PAGE and proteins were detected with α-p107, α-B55α, α-PP2A/A and α-PP2A/C antibodies. *m-Abs* and *p-Abs* indicate monoclonal and polyclonal antibodies, respectively (Jayadeva et al., 2010).

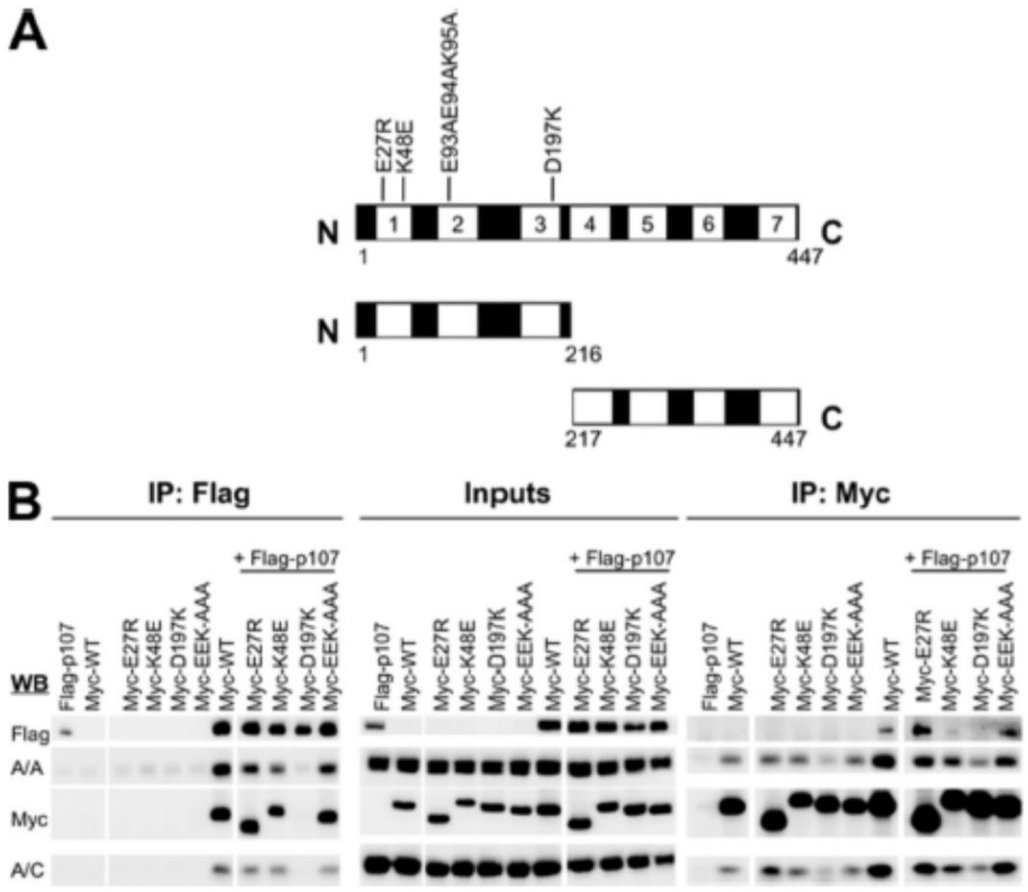

Fig. 2. B55α domains and residues required for binding to p107. (A) Structure of B55α and residues in its top acidic face that are important for dephosphorylation of the B55α substrate Tau. (B) B55α D197 is essential for the binding of p107. U-2 OS cells were co-transfected with Flag-p107 and the indicated Myc-B55α constructs. Cell lysates were immunoprecipitated with α-Flag and α-Myc antibodies and resolved via SDS-PAGE. Proteins were detected using α-Flag, α-Myc, α-PP2A/A and α-PP2A/C antibodies (Jayadeva et al., 2010).

<u>Research Project 12: Project Title and Purpose</u>

Are There Sex Differences in Kappa Opioid Receptor-Mediated Pharmacology? – Activation of the kappa opioid receptor (KOPR), one of the three types of opioid receptors (mu, delta and kappa), produces effects such as analgesia, sedation, dysphoria, water diuresis, antipruritic effects and attenuation of cocaine craving in addicts. Clinical studies have suggested sex differences in KOPR-induced analgesia. We have demonstrated that the selective KOPR agonist U50,488H produces higher levels of antinociception and sedation-like behavior in male than female guinea pigs. The underlying mechanisms are unclear. In the proposed studies, we will examine whether sex differences exist in KOPR distribution and signaling and alteration of neuronal circuitry activities by KOPR activation. We will investigate in vivo sex differences by measuring 1) receptor autoradiography, 2) G-protein coupling using [^{35}S]GTPγS autoradiography and 3) immunohistochemical labeling of *p44/42* MAP kinase activation induced by systemic KOPR agonist, U50,488H using intact male and female guinea pigs across the

estrous cycle. The guinea pig will be used as a model since its KOPR levels and distribution in brain resemble those of the human, unlike those of the rat and mouse.

Duration of Project

12/1/2010 – 6/30/2011

Project Overview

Specific Aim 1. Determine if there is a sex difference in KOPR distribution in the brain
<u>Hypothesis:</u> *Sex effects on KOPR distribution occur in a brain-region specific manner*
Experiment 1: Determine the affinity and total number of binding sites of [^{3}H]U69,593 binding to KOPR in male and female guinea pigs in phases of the estrous cycle associated with high and low levels of estrogen (proestrus and diestrus, respectively) using whole brain membranes.
Experiment 2: Examine the distribution and expression of KOPR in the brains of male, proestrus female and diestrus female guinea pigs by [^{3}H]U69,593 receptor autoradiography.

Specific Aim 2. Determine if there is a sex difference KOPR coupling to G-protein in the brain
<u>Hypothesis:</u> *Sex effects on KOPR coupling to G-protein occur in a brain-region specific manner*
Experiment 1: Examine the efficacy and potency of the KOPR agonist U50,488H in activating G-proteins by [^{35}S]GTPγS binding using whole brain membranes from male, proestrus female and diestrus female guinea pigs.
Experiment 2: Examine U50,488H-induced activation of G-proteins by [^{35}S]GTPγS binding autoradiography in the brains of male, proestrus female and diestrus female guinea pigs.

Specific Aim 3. Investigate whether there is a sex difference in KOPR agonist-induced modulation of neuronal circuitry in the brain
<u>Hypothesis:</u> *Activation or inhibition of neuronal activity by the KOPR agonist U50,488H is dependent on sex and brain region*
Experiment: Examine U50,488H-induced activation or inhibition of phosphorylation of p44/42 MAPK by immunohistochemistry on brains of male, proestrus female and diestrus female guinea pigs.

Principal Investigator

Lee-Yuan Liu-Chen, PhD
Professor
Department of Pharmacology
Center for Substance Abuse Research
Temple University School of Medicine
3420 N. Broad Street
Philadelphia, PA 19140

Other Participating Researchers

Yi-Ting Chiu – employed by Temple University

Expected Research Outcomes and Benefits

We expect that there will be brain region-specific sex differences in the distribution of KOPR, KOPR-G protein coupling and activation or inhibition of neuronal activities in different brain regions, which may correlate with the sex differences observed at the behavioral level.

The KOPR is a candidate for treatment of pain and cocaine abuse. Previous reports of sex differences in KOPR pharmacology may be mediated by gender and hormonal influence on organizational neural circuitry. However, very few studies have addressed whether the endogenous KOPR in the brain is affected by sex and sex hormones. Thus, elucidating whether neurobiological differences exist in endogenous KOPR distribution, signaling and neuronal circuits between males and females is crucial as these factors may potentially impact treatment outcomes. In the studies proposed here we aim to shed light on the basic neurobiological mechanism(s) underlying sex differences in KOPR pharmacology.

Summary of Research Completed

This study has been accepted for publication in *J.Pharm.Exp.Ther* (PM:21841040, Epub 8/12/2011).

Abstract
We examined if sex differences in KOPR pharmacology exists in guinea pigs, which are more similar to humans in the expression level and distribution of KOPR in the brain than rats and mice. The KOPR agonist U50,488H produced a dose-dependent increase in abnormal postures and immobility with greater effects in males than females. Males also showed greater U50,488H-induced antinociception in the paw pressure test than females. Pretreatment with KOPR antagonist norBNI blocked U50,488H-induced abnormal body postures and antinociception. In contrast, inhibition of cocaine-induced hyperactivity by U50,488H was more effective in females than males. Thus, sex differences in the effects of U50,488H are endpoint-dependent. We then examined if sex differences in KOPR level and KOPR-mediated G protein activation in brain regions may contribute to the observed differences using quantitative *in vitro* autoradiography of [^{3}H]U69,593 binding to the KOPR and U50,488H-stimulated [^{35}S]GTPγS binding. Compared to females, males exhibited greater [^{3}H]U69,593 binding in the deep layers of somatosensory and insular cortices, claustrum, endopiriform nucleus, periaqueductal gray, and substantial nigra. Concomitantly, U50,488H-stimulated [^{35}S]GTPγS binding was greater in males than females in the superficial and deep layers of somatosensory and insular cortices, caudate putamen, claustrum, medial geniculate nucleus and cerebellum. In contrast, compared to males, females showed greater U50,488H-stimulated [^{35}S]GTPγS binding in the dentate gyrus, and a trend of higher [^{35}S]GTPγS binding in the hypothalamus. These data demonstrate that males and females differ in KOPR expression and KOPR-mediated G-protein activation in distinct brain regions, which may contribute to the observed sex differences in KOPR-mediated pharmacology.

Sex difference in abnormal postures / immobility induced by KOPR activation
Activation of the KOPR is known to produce sedation and reduce locomotor activity. Since guinea pigs display low levels of baseline activity, we found that assessing reduced activity by

U50,488H in locomotor chambers yielded little information. During habituation, exploratory movement scores of guinea pigs are low and the animals habituate very quickly. However, in our pilot studies we observed that administration of U50,488H to guinea pigs produced a peculiar effect on their body posture (e.g., splayed limbs and body elongation) that occurred concomitantly with immobility. Immobility can be viewed as a sign of sedation. Based upon the changes in abnormal postures and immobility we observed, we developed a scoring system consisting of a rating scale between 0-5. We then compared the effects of U50,488H between male and female guinea pigs. Age-matched adult guinea pigs were injected with saline or U50,488H (2.5, 5 and 10 mg/kg, s.c.) at 0 min, placed into home cages and video-taped. Their posture changes were scored every 5 seconds and results are shown as score/min by adding up the scores from each 5-s bin (maximum 60). U50,488H caused a time- and dose-dependent increase in posture changes (leg splaying, body elongation) and immobility in both male and female guinea pigs. In males the effect of U50,488 (5 mg/kg) was blocked by pretreatment with the KOPR antagonist norBNI (5 mg/kg, i.p.), which was administered 18 hrs before U50,488H. These results indicate the effects are mediated by the KOPR.

To determine the magnitude of effect, we calculated the area under the curve (AUC) of the score/min data. Two-way ANOVA of AUC values revealed main effects of sex ($F_{(1, 43)} = 79.55$, $p < 0.0001$), dose ($F_{(2, 43)} = 132.90$, $p < 0.0001$) and an interaction sex x dose ($F_{(2,43)} = 17.01$, $p < 0.001$). Bonferroni *post-hoc* test revealed that the AUC values in males treated with U50,488H at 5 mg/kg and 10 mg/kg were significantly greater than females at the respective same dose ($p < 0.05$). NorBNI pretreatment significantly reduced the magnitude of effect of U50,488H ($p < 0.05$),

<u>Sex difference in KOPR-mediated antinociceptive effects</u>

We examined antinociception in the guinea pig using the paw pressure test, a mechanical pain assay. We found that males (Fig. 1A) showed greater responses to the same dose of U50,488H than females (Fig. 1B). Lower doses of U50,488H (2.5 and 1 mg/kg) were used since at 2.5 mg/kg, there was minimal postural change / immobility in both males and females and there was no sex difference. Data analysis by a three-way ANOVA (sex × dose × time) with time as a repeated measure revealed a significant difference between sexes ($F_{(1,49)} = 61.835$, $p < 0.001$), dose ($F_{(2,47)} =11.770$, $p < 0.001$) and time ($F_{(10,470)} = 18.429$, $p < 0.001$) and a significant interaction between sex × dose ($F_{(2, 47)} = 0.643$, $p = 0.05$). Results of Bonferroni *post-hoc* tests showed significant increases in analgesymeter scores in males at 15 and 30 min after treatment with 1 mg/kg U50, 488H and at 15, 30, 45 and 60 min after 2.5 mg/kg U50,488H. In females, only 2.5 mg/kg U50,488H produced significant antinociceptive effects at 15 and 45 min after injection. In addition, in males we found that nor-BNI (10 mg/kg) pretreatment blocked the antinociceptive effects of 2.5 mg/kg U50,488H observed at 45 and 60 min.

AUC values of data from Fig. 1A and 1B were determined to compare the magnitude of effect. As shown in Fig. 1C, males showed a significant antinociceptive response to U50,488H at 1 and 2.5 mg/kg, while females displayed antinociception only at 2.5 mg/kg. Specifically, two-way ANOVA revealed a main effect of sex ($F_{(1,48)} = 66.71$, $p < 0.0001$) and dose ($F_{(2,48)} = 15.43$, $p < 0.0001$) and an interaction between sex × dose, ($F_{(2,48)} = 4.33$, $p < 0.05$). NorBNI (10 mg/kg) pretreatment blocked the effects of U50,488H (2.5 mg/kg) in males. In addition, baseline values,

i.e., absolute weight thresholds, were significantly lower in females. These results clearly indicate that male guinea pigs have greater antinociceptive responses to U50,488H than females.

Sex difference in KOPR blockade of cocaine-induced hyperactivity

We assessed the effects of U50,488H (1 mg/kg) on cocaine-induced ambulation and stereotypy. We chose to use this dose since (1) at 2.5 mg/kg animals displayed abnormal body postures and immobility which may confound locomotor responses and (2) clear sex differences were found in the antinociceptive assay at 1 mg/kg (males > females, see Fig. 1). Cocaine significantly increased locomotor activity (ambulation and stereotypy) in both males and females (Fig. 2A and B). Two-way ANOVA of total ambulation scores revealed main effects of sex ($F_{(1,42)} = 6.65$, $p < 0.05$) and drug treatment ($F_{(2,42)} = 17.78$, $p < 0.001$), and an interaction sex × drug treatment ($F_{(1,2,42)} = 7.78$, $p < 0.005$). Cocaine induced a significantly greater increase in ambulation in females than males (Fig. 2A). In addition, in females, but not males, U50,488H pretreatment significantly reduced cocaine-induced ambulation scores.

For stereotypy, two-way ANOVA revealed main effects of sex ($F_{(1,42)} = 7.71$, $p < 0.01$) and drug treatment ($F_{(2,42)} = 18.80$, $p < 0.01$) but no significant interaction sex × drug treatment ($F_{(2,42)} = 1.61$, $p > 0.05$). Overall, regardless of drug treatment females displayed significantly greater stereotypic behavior than males. Cocaine treatment increased stereotypy in males and females. In addition, U50,488H blocked cocaine-induced stereotypy in both sexes.

Sex Differences in [^{3}H]U69,593 binding to the KOPR

We compared the levels and distribution of [^{3}H]U69,593 binding to KOPR between male and female guinea pig brains. Representative pseudo-color autoradiograms are shown in Fig. 3. In general, male and female guinea pigs displayed similar regional distribution (Fig. 3). Quantitation of specific [^{3}H]U69,593 binding was obtained by measuring the density of autoradiograms in regions of interest. Table 2 shows the analysis of specific [^{3}H]U69,593 binding. Males exhibit significantly higher [^{3}H]U69,593 binding than females in the following brain regions: deep layers of somatosensory cortex and insular cortex, claustrum, endopiriform nucleus, periaqueductal gray, and substantial nigra. However, in any other brain regions we did not observe any significant sex difference in [^{3}H]U69,593 binding.

Sex Differences in U50,488H-stimulated [^{35}S]GTPγS binding

U50,488H-stimulated [^{35}S]GTPγS binding was compared between male and female guinea pig brains. Representative pseudo-color autoradiograms of U50,488H-stimulated [^{35}S]GTPγS binding are shown in Fig. 4. Males and females displayed similar neuroanatomical distribution of U50,488H-stimulated [^{35}S]GTPγS binding. Table 3 shows the analysis of basal and net U50,488H-stimulated [^{35}S]GTPγS binding. There is no difference between males and females in basal levels of binding, but there are large regional differences. U50,488H-stimulated [^{35}S]GTPγS binding was significantly greater in males than females in several brain regions, which include superficial and deep layers of somatosensory cortex and insular cortex, caudate putamen, claustrum, medial geniculate nucleus and cerebellum. In contrast, in the dentate gyrus of the hippocampus, females exhibited significantly higher U50,488H-stimulated [^{35}S]GTPγS binding than males. In addition, females exhibited a trend of higher levels in the hypothalamus, but it did not reach statistical significance (P = 0.09).

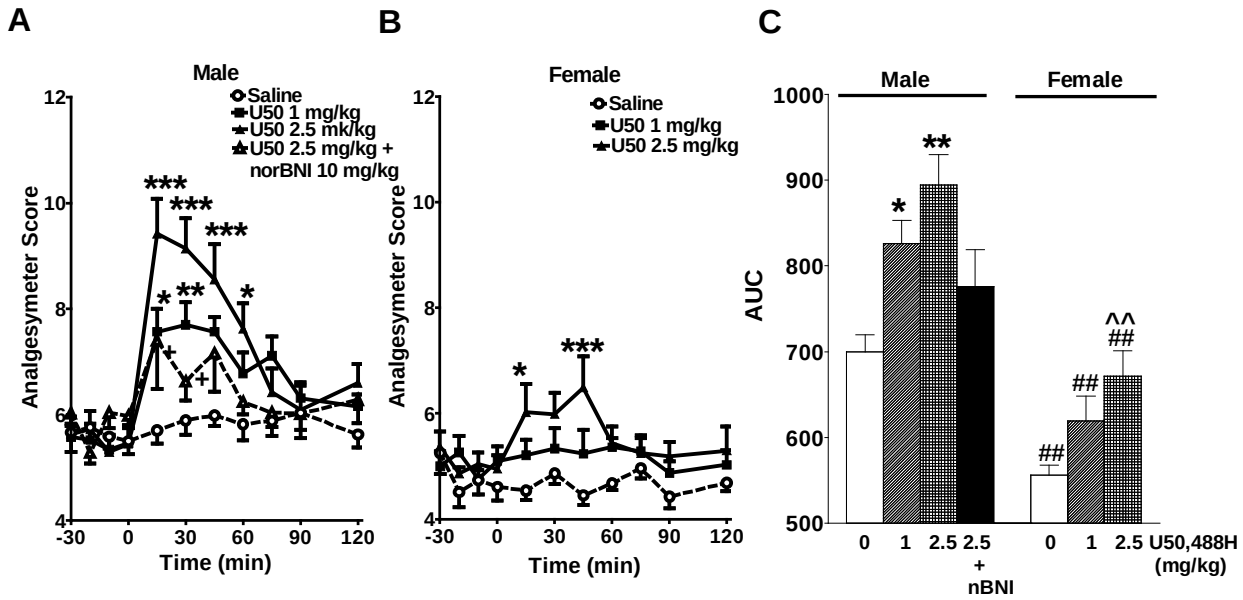

Figure 1. U50,488H-induced antinociception in the paw pressure test is dose-, time-, and sex-dependent. The paw pressure test was performed as described in Methods. Four baseline nociceptive threshold responses were recorded in 10-min intervals prior to drug treatment (-30, -20, -10 and 0 min). Immediately after the last baseline measurement, animals were then treated s.c. with saline or U50,488H at indicated doses at time 0 and nociceptive thresholds were determined in 15-min intervals for 90 min and then at 120 min. Data are plotted as the mean ± SEM analgesymeter score for (A) male (n=8-12) and (B) female (n=8) guinea pigs. In males norBNI (10 mg/kg, open triangle, dotted line) was given 18 hours prior to U50,488H (2.5 mg/kg). Mean AUC values (± SEM) is shown in (C). *** $p < 0.001$, ** $p < 0.01$ and * $p < 0.05$ vs saline; ^^ $p < 0.01$ vs saline same sex. + $p < 0.05$, 2.5 mg/kg U50,488H vs 2.5 mg/kg U50,488H + norBNI at same time point. ## $p < 0.01$ vs male same dose.

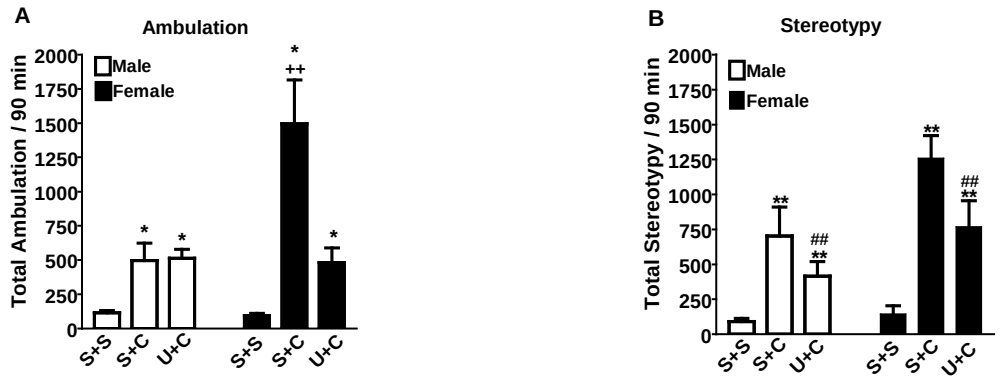

Figure 2. Effects of U50,488H on cocaine-induced hyperactivity are sex-dependent. Locomotor activity was monitored for 90 min after animals were treated with saline (1ml/kg) or 20 mg/kg cocaine (i.p.). Each value represents the total (A) ambulation counts or (B) stereotypy measured over the 90-min period in males (filled bar) and females (open bars). Data are expressed as mean + SEM (n=8/treatment group).

In (A) * $p < 0.05$ saline-cocaine or U50,488H-cocaine vs saline-saline treatment and ++ $p < 0.01$ female saline-cocaine vs all other groups. In (B) ** $p < 0.01$, saline-cocaine or U50,488-cocaine vs saline-saline; ## $p < 0.01$, saline-cocaine vs U50,488-cocaine. Saline-Saline, S+S ; Saline-Cocaine, S+C ; U50,488H-Cocaine, U+C

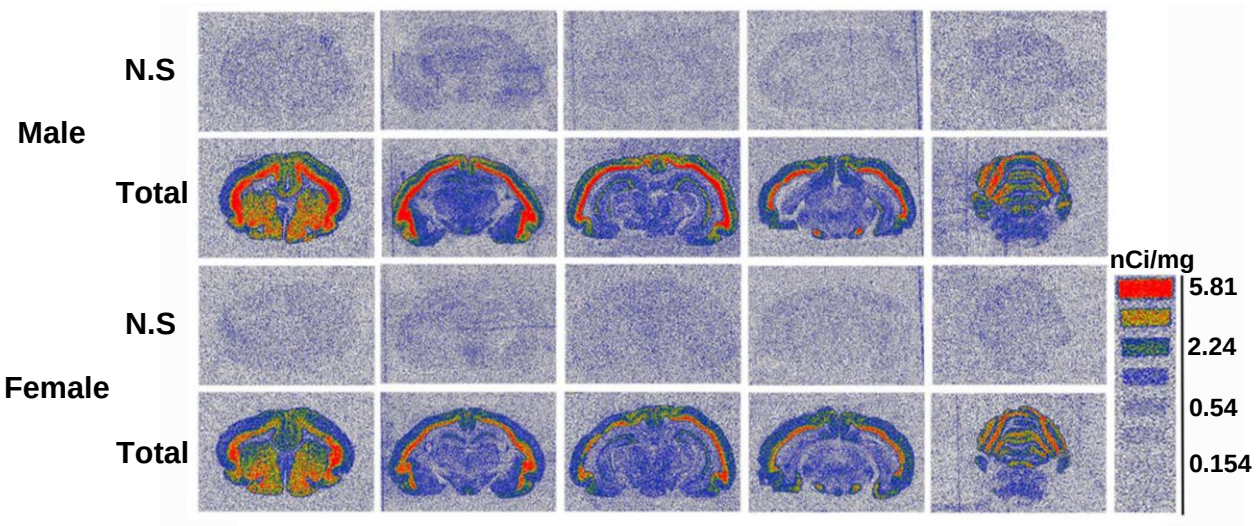

Figure 3. Psedudo-color autoradiograms of [^{3}H]U69593 (~5 nM) binding to the kappa opioid receptor in coronal brain sections of male and female guinea pig brain. Sections were incubated with ~5 nM [3H]U69,593 for 1 hour at 25°C, washed, dried and exposed to tritium-sensitive phosphor screens. Non-specific binding (N.S) measured in the presence of 10 μM naloxone. Exposure time was 3 weeks. The color bars are pseudo-color representation of black and white screen images in fmol/mg tissue equivalents. Male and female sections were processed in parallel throughout binding experiments and for development of autoradiograms.

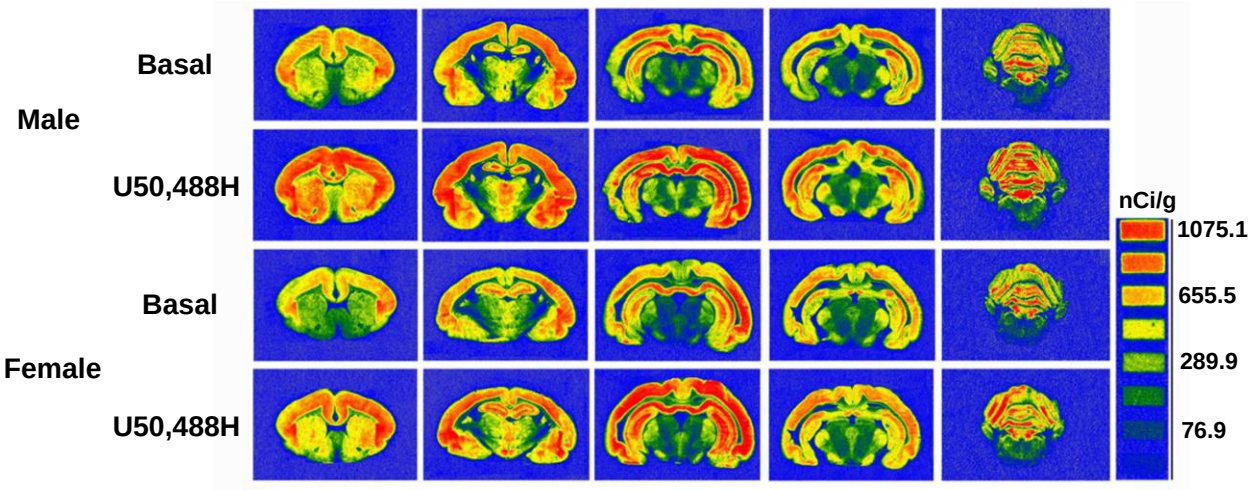

Figure 4. Pseudo-color autoradiograms of of U50,488H-stimulated [^{35}S]GTPγS binding in coronal sections of male and female guinea pig brain. Sections were incubated with ~0.04 nM [^{35}S]GTPγS and 2 mM GDP, in the absence (Basal) or presence of 10 μM of U50,488H. Exposure time was 48 hours. The color bars are pseudo-color representations of black and white screen images in nCi/g tissue equivalents. Male and female sections were processed in parallel throughout [^{35}S]GTPγS binding experiments and for development of autoradiograms.

Research Project 13: Project Title and Purpose

Enhancing Stem Cell Engraftment and New Myocyte Formation in the Damaged Heart – The purpose of this study is to develop and test novel approaches to enhance the survival and engraftment of cardiac stem cells in the injured heart. We have characterized a population of resident cardiac stem cells in the normal heart and have shown that these cells have the capacity to differentiate into new cardiac myocytes. In the proposed research we will modify the properties of these stem cells so that they have enhanced survival in the hostile environment of the injured heart. We will also modify the stem cells so that they have an enhanced ability to electrically couple to cardiac myocytes. The purpose of the research is to test the idea that enhancing coupling increases survival and induces differentiation.

Anticipated Duration of Project

7/1/2011 – 6/30/2012

Project Overview

The objectives of the proposed experiments are to develop a novel approach to modify cardiac stem cells so that they have enhanced survival in the injured heart, and they then differentiate into new cardiac myocytes and vascular tissue.

Specific Aim: This study will determine if enhancing (or reducing) the coupling between resident cardiac stem/progenitor (CS/PCs) cells and myocytes in the damaged heart increases CS/PC survival and the generation of new myocytes, thereby improving cardiac function. Feline CS/PCs with enhanced or suppressed ability to electrically couple to myocytes will be injected

into a myocardial infarction model. CS/PC survival, differentiation into new myocytes, functional maturity and alterations in cardiac function will be measured. Mouse CS/PCs with enhanced or suppressed (transgenic or KO approaches) coupling capabilities will be injected into a mouse heart after myocardial infarction. CS/PC survival, differentiation into new myocytes, functional maturity and alterations in cardiac function will be measured. Feline and mouse CS/PCs in co-culture with NRVMs will be studied in a hypoxic environment to determine if this environment reduces electrical coupling and new myocyte formation. These studies will test if mutant Cx43 constructs that do not uncouple in hypoxic environments can rescue CS/PC mediated new myocyte formation.

Principal Investigator

Steven R. Houser, PhD
Professor and Chair, Cardiovascular Research
Temple University
3500 North Broad Street
MERB 1041
Philadelphia, PA 19140

Other Participating Researchers

Jason Duran, BA – employed by Temple University

Expected Research Outcomes and Benefits

Ischemic heart disease and hypertension induce cardiac dysfunction and ultimately cause congestive heart failure (CHF). The cellular and molecular factors that initiate cardiac dysfunction in CHF and drive its progression are still not fully understood. Disease-induced myocyte death (apoptosis and necrosis) and a resulting decrease in the number of functional cardiac myocytes is thought to be a major contributor to depressed cardiac pump function in heart failure. Myocyte death and the associated cardiac remodeling (dilation of the ventricle and the resulting increase in cardiac wall stress) lead to a heart that is incapable of pumping normal quantities of blood. Current approaches to improve the function of the damaged heart produce only modest improvement in cardiac function and life expectancy. Standard CHF therapies are not directed at improving cardiac function by increasing the number of myocytes. With the advent of cell therapy, there is hope that appropriate use of stem cells might improve outcomes for individuals with depressed cardiac performance by increasing the number of functioning cardiac myocytes. This idea has been tested in a number of preclinical animal experiments and in early stage human clinical trials. Some of these early clinical trials suggest that stem cell therapy can improve cardiac performance. However, the results have been somewhat variable and the bases of improved cardiac function are still highly controversial. Most investigators would agree that there is ample room for improvement in cell therapy for cardiac disease. In particular, those factors that determine CS/PC survival and differentiation into functional myocardium are still not well established. Our proposed research will examine fundamental aspects of new myocyte generation specifically related to Ca^{2+} signaling, with the hope that the new knowledge and approaches we develop will lead to improved cell therapy for the damaged heart. We hope to

develop a novel cell therapy approach that can be translated into a therapy for patients with ischemic heart disease.

Summary of Research Completed

This project has been delayed and therefore no research to report. New start date 07/01/2011.

Research Project 14: Project Title and Purpose

Neural Effects of Acute Traumatic Brain Injury – The purpose of this research is to investigate how brain neural activity is altered in response to traumatic brain injury. Whereas other researchers have investigated both short and long term neural behavior in brain injury patients, there has been no systematic study of what changes occur in the moments immediately following the insult or how these changes vary as a function of the severity of the injury. That knowledge is a crucial missing link in understanding the mechanisms of brain injury; a deeper understanding will lead to enhanced strategies for prevention, detection, and treatment.

Anticipated Duration of Project

12/1/2010 – 6/30/2012

Project Overview

This project will initiate a long-term multi-PI collaboration whose purpose will be to elucidate the mechanisms of traumatic brain injury by analyzing electroencephalographic (EEG) data recorded during and immediately after insult. This work represents a truly synergistic interaction between the collaborating faculty in that it combines three areas of expertise, all of which are necessary for the successful execution of the research. These three areas are neural data acquisition and signal processing, biomechanics of traumatic impact injuries, and neural anatomy and histology. The project will yield preliminary data that will suggest new directions for the PIs to pursue for future funding; the PIs expect to pursue both federal (NIH) and foundation (professional sports associations) follow-up funding.

Specific Aim: The main hypothesis of this study is that EEG signals will show deterministic changes due to acute head trauma. Such changes can then be used to assess the severity of the injury. This study will have two specific aims:

Aim 1: Investigating EEG signals in rats before, during, and after head trauma. Adult rats will be instrumented with EEG electrodes and a wireless transmitter. The instrumented rats will undergo high linear deceleration brain injuries. The EEG signals will be recorded before, during, and after the impact, and their changes will be evaluated.

Aim 2: Investigating brain pathology after impact and determining its correlation to the EEG results found in Aim 1. Rat vital signs and general behavior will be monitored for 48 hours post trauma. Rat brains will be subsequently harvested and evaluated for hematoma, contusion, and axonal injury.

Principal Investigator

Iyad Obeid, PhD
Assistant Professor
Temple University
1947 N. 12th Street
Philadelphia, PA 19122

Other Participating Researchers

Kurosh Darvish, PhD, Mary F. Barbe, PhD – employed by Temple University

Expected Research Outcomes and Benefits

The significance of traumatic brain injury (TBI) as a leading cause of worldwide mortality and long-term morbidity is well established. While the importance of TBI has generated considerable attention and insight into the complexity of the problem has been gained, a comprehensive understanding of the injury mechanisms and tolerances still eludes researchers.

A principal tool for studying TBI is the electroencephalogram (EEG), in which electrodes record the aggregate electrical signatures from populations of spatially localized neurons. In humans, EEG is typically recorded from the scalp surface and is therefore non-invasive and hence often the measurement of choice for acute TBI patients in intensive care. For this reason, most studies of TBI in animals have also focused on the significance and analysis of EEG signals.

The expected outcome of this research is that the PIs will develop new tools for studying the time course of neural degeneration in the immediate aftermath of traumatic brain injury. These new research tools will allow the PIs to initiate a long-term research agenda that will lead to a deeper understanding of (a) the mechanics of brain injury (b) the time-series of neural degeneration events associated with TBI and (c) the correlation of neural degeneration with behavioral degeneration. Specifically, the PIs will use the tools generated in this project to study how series of small, relatively minor head impacts can accumulate over time to produce substantial brain damage. This is an important area of increased interest to the medical community, especially as researchers become increasingly aware of the risk of repeated minor brain trauma experienced by contact-sport athletes ranging from youths to professionals.

Summary of Research Completed

The project has been initiated and several important milestones have already been achieved. Our goal has been to establish a new research model for studying the cumulative effects of minor traumatic brain injury episodes in rats. Specifically, we seek to correlate changes in electroencephalogram (EEG) signals in the rat with accumulated brain injury as measured by post-mortem histology. The PADOH funds became available to us in December 2010, so this Summary discusses a research period covering approximately six months.

Most of the proposed work relating to methodology has been completed. The centerpiece of this effort has been the acquisition of the rat EEG data acquisition system from Data Sciences International and our subsequent training on implantation procedures, data collection and analysis, and animal handling techniques. We have purchased two F40-EET implantable transmitters, as well as a Physiotel Receiver, a Data Exchange Matrix, and the Dataquest ART signal acquisition system. Collectively, these pieces allow us to record EEG information from unencumbered rats as they move freely within their enclosures. To date, six rats have been implanted for short duration proof-of-concept studies.

Each rat was anesthetized with ketamine and xylazine, and the head, neck, and back was then clipped to remove the hair and prepared with a povidone-iodine (Betadine) or chlorhexidine (Nolvasan) scrub followed by an alcohol rinse. Two incisions are made: a 1cm midline incision at the scalp centered on top of the skull, and a 2cm incision in the back. A small subcutaneous pocket is created at the back incision to house the transmitter assembly. The transmitter assembly is hardwired to four flexible electrode wires. A subcutaneous tunnel is made between the two incisions. Four transmitter wires are passed through the tunnel from the transmitter assembly to the head. The scalp is retracted to expose the skull and identify lambda and bregma landmarks. Four holes 2mm holes are drilled through the skull using a small handheld drill fitted with a surgical-grade drill bit. The first pair of holes is drilled 2mm on either side of the midline, 3mm posterior to bregma. The second pair of holes is drilled 5mm posterior to bregma and 5mm on either side of the midline.

A single EEG electrode is introduced into the brain through each drill hole. Electrodes in the first pair of holes sit on the surface of the brain, whereas electrodes in the second set of holes are inserted to a depth of 6mm in order to record bilaterally from the ventral hippocampus. The electrodes are secured in place with surgical screws that are sized specifically to match the drill bit gauge. The skin at both incisions is sutured closed.

Owing to the design of the EEG data acquisition system, the process of making recordings is completely passive from the perspective of the rat. The rat's plexiglass enclosure is placed on top of a metallic recording pad that contains all the necessary electronics for interrogating the transmitter implanted within the rat. Data is streamed wirelessly from the implanted transmitter, into the recording pad, and is then passed to a personal computer where it is stored. The rat is not restrained or limited in any manner; it can move normally within its cage throughout the recording session.

EEG sessions have typically lasted for 15 minutes each and were made immediately after implantation and again after impact (see below). Of the six implanted animals, only two were also subject to impact testing.

A newly developed test facility at the Temple Biomechanics Laboratory features a linear impact carriage (Figure 1) capable of generating traumatic brain injuries with deceleration rates up to 300G with as low as 10ms duration. The linear impact carriage system consists of two 6m parallel tracks, one active, driven by an electric servo motor, and one passive with a freely sliding carriage that is pushed forward by the active track. The anesthetized animal is positioned on the freely sliding carriage and is immobilized. The animal is then accelerated at 4G to 13m/s

constant velocity and is decelerated when the carriage hits a shock absorber at the end of the track and is stopped by a latch system. No direct impact is applied to the head and any TBI is the result of pure acceleration. The shape of the acceleration pulse can be adjusted by the damping characteristics of the shock absorber, initial velocity, and total mass of the carriage.

We also developed a method for restraining the rat during impact testing by positioning the anesthetized animal between cast clear silicone blocks with a negative space that fit to the animal body. Animals were positioned laterally with impact force in the superior-inferior direction, which will minimize compression of tissues during the impact on each other that could result in additional internal injuries.

To date, six rats have been tested in the impact device (without the implanted EEG). Of these, two received multiple impacts (3 x 80G) and the remainder received single impacts (1 x 80G). These pilot data have shown us that the multiple-blow configuration is sufficient to consistently kill the rat on impact, whereas the single-blow configuration appears to be non-fatal. These data are important because it is vital that we learn to differentiate between mild and severe episodes of brain injury in the deceleration rat model. With an upper bound established, we are now able to work backwards and elucidate impact levels for moderate or mild traumatic brain injury.

In summary, the following milestones have been achieved during the first six months of this research:

- Purchase of rat EEG data acquisition system and training in implantation protocol.
- Pilot study comprising implantation and recording of baseline EEG signals from six rats.
- Completion and testing of the linear impact device, including silicone mold for rat restraint.
- Pilot study comprising linear impact testing on six rats.

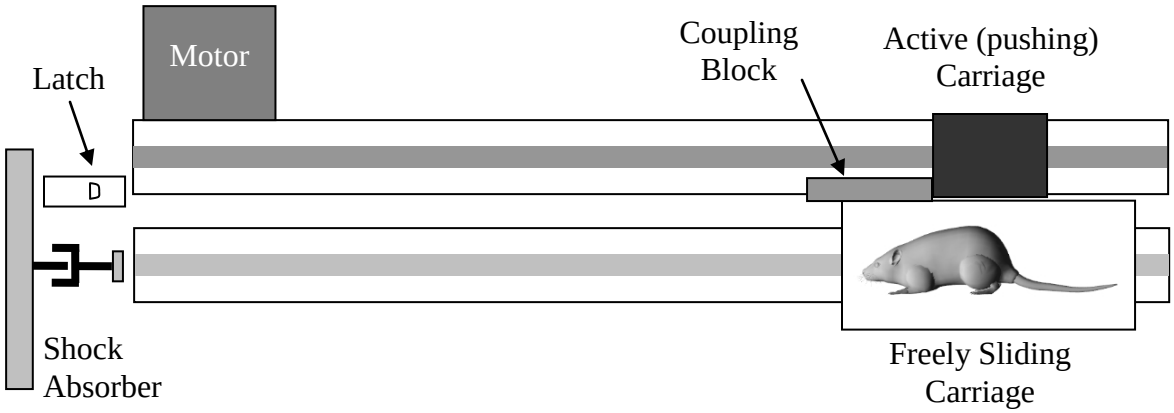

Figure 1: Schematic diagram of the experimental setup with linear impact carriage to study acceleration TBI.